σ_2-Adaptin Facilitates Basal Synaptic Transmission and Is Required for Regenerating Endo-Exo Cycling Pool Under High-Frequency Nerve Stimulation in *Drosophila*

Saumitra Dey Choudhury,*,[1] Zeeshan Mushtaq,*,[1] Suneel Reddy-Alla,[†] Sruthi S. Balakrishnan,[‡] Rajan S. Thakur,[§] Kozhalmannom S. Krishnan,[‡,2] Padinjat Raghu,[‡] Mani Ramaswami,[‡,] and Vimlesh Kumar*,[3]**

*Department of Biological Sciences, Indian Institute of Science Education and Research (IISER) Bhopal, Govindpura-Bhopal 462 023, Madhya Pradesh, India, [†]Institute for Biology/Genetics, Free University of Berlin, 14195 Berlin, Germany, [‡]National Center for Biological Sciences, Tata Institute of Fundamental Research, Bangalore 560 065, India, [§]Shanmugha Arts, Science,Technology and Research Academy, Thanjavar 613 401, India, and **Trinity College Institute of Neuroscience (TCIN), Trinity College Dublin, University of Dublin, Dublin 2, Ireland

ORCID IDs: 0000-0001-8828-4551 (S.D.C.); 0000-0003-3416-2289 (Z.M.); 0000-0003-2206-4905 (V.K.)

ABSTRACT The functional requirement of adapter protein 2 (AP2) complex in synaptic membrane retrieval by clathrin-mediated endocytosis is not fully understood. Here we isolated and functionally characterized a mutation that dramatically altered synaptic development. Based on the aberrant neuromuscular junction (NMJ) synapse, we named this mutation *angur* (a Hindi word meaning "grapes"). Loss-of-function alleles of *angur* show more than twofold overgrowth in bouton numbers and a dramatic decrease in bouton size. We mapped the *angur* mutation to σ_2-adaptin, the smallest subunit of the AP2 complex. Reducing the neuronal level of any of the subunits of the AP2 complex or disrupting AP2 complex assembly in neurons phenocopied the σ_2-adaptin mutation. Genetic perturbation of σ_2-adaptin in neurons leads to a reversible temperature-sensitive paralysis at 38°. Electrophysiological analysis of the mutants revealed reduced evoked junction potentials and quantal content. Interestingly, high-frequency nerve stimulation caused prolonged synaptic fatigue at the NMJs. The synaptic levels of subunits of the AP2 complex and clathrin, but not other endocytic proteins, were reduced in the mutants. Moreover, bone morphogenetic protein (BMP)/transforming growth factor β (TGFβ) signaling was altered in these mutants and was restored by normalizing σ_2-adaptin in neurons. Thus, our data suggest that (1) while σ_2-adaptin facilitates synaptic vesicle (SV) recycling for basal synaptic transmission, its activity is also required for regenerating SVs during high-frequency nerve stimulation, and (2) σ_2-adaptin regulates NMJ morphology by attenuating TGFβ signaling.

KEYWORDS *Drosophila*; *angur*; synapse; physiology; pMAD

SYNAPTIC transmission requires fusion of synaptic vesicles (SVs) at the active zones followed by their efficient retrieval and recycling through endocytic mechanisms (Heuser and Reese 1973; Jahn and Sudhof 1994). Retrieval and sorting of membrane lipids and vesicular proteins at the synapse are mediated by a well-orchestrated and coordinated action of several adapter and endocytic proteins (Stimson *et al.* 2001; Rikhy *et al.* 2002; Verstreken *et al.* 2002; Koh *et al.* 2004; Marie *et al.* 2004). Clathrin-mediated endocytosis (CME) is the primary pathway operative at the synapses for membrane retrieval (Granseth *et al.* 2006, 2007; Heerssen *et al.* 2008; Dittman and Ryan 2009; McMahon and Boucrot 2011; Saheki and De Camilli 2012). Genetic analysis of the components of the CME pathway in *Caenorhabditis elegans* and *Drosophila* has revealed that this pathway is required for SV re-formation, and in many cases, blocking CME at synapses

doi: 10.1534/genetics.115.183863
Manuscript received October 23, 2015; accepted for publication February 21, 2016; published Early Online February 23, 2016.
Supplemental material is available online at www.genetics.org/lookup/suppl/doi:10.1534/genetics.115.183863/-/DC1.
[1]These authors contributed equally to this work.
[2]Deceased.
[3]Corresponding author: Indian Institute of Science Education and Research, ITI Building, Govindpura, Bhopal, 462 023, Madhya Pradesh, India. E-mail: vimlesh@iiserb.ac.in

results in temperature-sensitive paralysis (Gonzalez-Gaitan and Jackle 1997; Zhang *et al.* 1998; Stimson *et al.* 2001; Koh *et al.* 2004, 2007; Sato *et al.* 2009). Additionally, CME plays a crucial role in regulating synaptic morphology (Rikhy *et al.* 2002; Koh *et al.* 2004, 2007; Dickman *et al.* 2006). At *Drosophila* NMJs, blocking CME results in enhanced bone morphogenetic protein (BMP) signaling and affects synaptic growth (Coyle *et al.* 2004; O'Connor-Giles *et al.* 2008).

The heterotetrameric adapter protein 2 (AP2) complex is a major effector of the CME pathway. AP2 serves as a major hub for a large number of molecular interactions and links plasma membrane, cargo/signaling molecules, clathrin, and accessory proteins in the CME pathway (Traub 2003; Schmid and McMahon 2007) and hence can directly influence synaptic signaling. The AP2 complex is pseudo-asymmetric and contains four subunits—one each of large α and β_2 subunits, one medium μ_2 subunit, and a small σ_2 subunit (Matsui and Kirchhausen 1990; Collins *et al.* 2002; Traub 2003). Depletion of clathrin or its major adapter, AP2, in either *Drosophila* or mammalian central synapses results in accumulation of endosome-like vacuoles and reduction of SVs, suggesting that CME may not be essential for membrane retrieval (Heerssen *et al.* 2008; Gu *et al.* 2013; Kononenko *et al.* 2014). Similarly, genetic perturbation of μ_2-adaptin or α-adaptin shows only mild defects in vesicle biogenesis at *C. elegans* synapses, but simultaneous loss of both adaptins leads to severely compromised SV biogenesis and accumulation of large vacuoles at nerve terminals (Kim and Ryan 2009; Gu *et al.* 2013). While *Drosophila* loss-of-function mutations in α-adaptin are embryonic lethal, hypomorphic mutants exhibit reduced FM1-43 uptake, suggesting a compromised endocytosis in these mutants (Gonzalez-Gaitan and Jackle 1997). Whether reduced endocytosis reflects a defect in membrane retrieval or a defect in SV biogenesis remains unclear. Moreover, the consequences of AP2 reduction on synaptic morphology and physiology remain unknown.

Here we present an analysis of *Drosophila* σ_2-adaptin in the context of regulating NMJ morphological plasticity and physiology. We first identified a mutation that dramatically altered NMJ morphology. Next, we mapped this mutation to σ_2-adaptin by deficiency mapping. We show that AP2-dependent vesicle endocytosis regulates both synaptic growth and transmitter release. The AP2 complex is a heterotetramer, and our studies in *Drosophila* show that the four subunits are obligate partners of each other and are required for a functional AP2 complex (Collins *et al.* 2002). This finding is in contrast to the hemicomplex model in *C. elegans*, in which α/σ_2 and β_2/μ_2 can sustain the function, if any one of the subunits is mutated (Gu *et al.* 2013). We find that loss of AP2 disrupts stable microtubule loops of the presynaptic cytoskeleton and exacerbates growth signaling through the phosphorylated Mothers Against Decapentaplegic (pMAD) pathway, suggesting that normal AP2 constrains the TGFβ signaling module. Reducing σ_2-adaptin level results in synaptic fatigue at the larval NMJ synapses during high-frequency stimulation and causes temperature-sensitive paralysis in adults. Based on these results, we suggest that AP2 is essential for attenuating synaptic growth signaling mediated by the TGFβ pathway in addition to its requirement in regenerating SVs under high-frequency nerve firing.

Materials and Methods

Fly genetics

All the flies were maintained at 25° in standard corn meal medium containing sucrose, agar, and yeast granules. Flies for RNA interference (RNAi) experiments were reared at 28°. *angur* alleles were obtained as a second mutation through *P*-element mobilization of $synd^{EP877}/TM6B$, *Tb*. All deficiency lines and mutants including the *P*-element insertion line $AP2\sigma^{KG02457}$ (BL13478) were obtained from the Bloomington Drosophila Stock Center at Indiana University. Mutant *σ_2-adaptin* and control and rescue larvae were grown in noncrowded conditions on apple agar plates with a yeast paste dollop. All controls used in this study were w^{1118} unless stated otherwise.

Mutant eye clones

We generated $angur^7$, *FRT82B/TM6*, *Tb* stock by recombining $angur^7$ with *FRT82B* (BL2035). This recombinant was crossed to *yw*; *ey GAL4 UAS-FLP*; *FRT82BGMR-hid 3R CL3R/TM6*, *Tb* to generate flies with eyes homozygous for $angur^7$. These mutant eye clones thus were generated using the *EGUF-hid* technique (Stowers and Schwarz 1999). The eye rescue construct $angur^7$, *FRT82B*, *UAS-AP2σ/TM6*, *Tb* was similarly generated using standard fly genetics.

Electroretinograms (ERGs)

Flies were anesthetized and immobilized at the end of a disposable pipette tip using a drop of clear nail varnish. Recordings were done using glass microelectrodes filled with 0.8% w/v NaCl solution. Voltage changes were recorded between the surface of the eye and an electrode placed on the thorax. Following fixing and positioning, flies were dark adapted for 5 min. ERGs were recorded with 2-sec flashes of green light as a stimulus. Stimulating light was delivered from a light-emitting diode (LED) light source to within 5 mm of the fly's eye through a fiber-optic guide. Calibrated neutral-density filters were used to vary the intensity of the light source. Voltage changes were amplified using a DAM50 amplifier (WPI) and recorded using pCLAMP 10.4. Analysis of traces was performed using Clampfit 10.4 (Axon Laboratories).

Transgene rescue

The σ_2-adaptin ORF was amplified and cloned in pUAST vector. The transgenic flies were generated by the Fly Facility of the Centre for Cellular and Molecular Platforms–National Centre for Biological Sciences (CCAMP-NCBS), Bangalore, India. The transgene was expressed in a tissue-specific manner using the bipartite UAS-Gal4 system (Brand and Perrimon 1993). The Gal4 drivers used were the ubiquitous *actin5C*-Gal4 and

the pan-neuronal *elav*^{C155}-Gal4. All genetic combinations and recombinants were made using standard *Drosophila* genetics. The rescue experiments were performed at 25°.

RNAi knockdown experiments

The following RNAi lines were obtained from the Bloomington Drosophila Stock Center at Indiana University: RNAi α-adaptin (BL32866), RNAi β_2-adaptin (BL28328), RNAi μ_2-adaptin (BL28040), RNAi σ_2-adaptin (BL27322), and RNAi PI4KIIIα (BL35256). All these RNAi lines were crossed to appropriate Gal4 drivers, and progeny were reared at 28°. Where lethality was observed at 28 or 25°, as in the case of α-adaptin and PI4KIIIα RNAi, the animals were raised at 18°.

Reverse transcription PCR (RT-PCR) and transcript quantification by real-time quantitative PCR (RT-qPCR)

Total RNA was isolated from larval fillets of the mentioned genotypes using Qiagen's RNA extraction kit as per the manufacturer's instructions. The total amount of RNA from each genotype was quantified using a Nanodrop (Thermo Scientific), and 50 ng of RNA was taken to synthesize the first-strand complementary DNA (cDNA) using SuperScipt II (Life Technologies). One-tenth volume of the reaction mix was subjected to RT-qPCR with the 7500 Cycler (Applied Biosystems). The sequences of primers used in this study are listed in Supplemental Material, Table S2.

The primers used for the analysis were designed using the Primer-BLAST tool from the National Center for Biotechnology Information (NCBI). Cycling conditions during RT-qPCR were as follows: 50° for 2 min, 95° for 10 min, and 40 cycles at 95° for 15 sec, followed by 60° for 1 min. SYBR Green was used for the detection of amplicons with a final primer concentration of 200 nM. Individual RT-qPCR runs were performed in triplicate. The fold change was calculated using $2^{-\Delta(\Delta Ct)}$.

Brightfield imaging

Three-day-old flies were anesthetized with ether, and images were captured using a Leica M205FA Stereo Zoom Microscope.

Scanning electron microscopy

Three-day-old flies were immersed in fixative (1% glutaraldehyde, 1% formaldehyde, and 1 M sodium cacodylate, pH 7.2) for 2 hr, followed by rinsing in water and dehydration via an ethanol series. The samples then were critical point dried and sputter coated (Wolff 2011). The flies were mounted on carbon conductive tabs stuck on aluminum stubs, and images were captured using a Zeiss scanning electron microscope.

Transmission electron microscopy (TEM)

Adult eyes of control animals, *angur*^{7} mutant mitotic clones, and rescue genotype animals were prepared for TEM by fixing the eyes for 2 hr at 25° in 2.5% each of paraformaldehyde and glutaraldehyde in 0.1 M cacodylic acid (pH 7.3) containing 7 mM $CaCl_2$. The eyes were postfixed in 2% OsO_4 for 2 hr at 4°, as described previously (Meinertzhagen 1996). The samples were visualized at 120 kV using a Zeiss LIBRA 120 transmission electron microscope.

Antibodies and immunocytochemistry

Antibodies against *Drosophila* α- and β_2-adaptin were raised in rabbits. Briefly, the C-terminal region corresponding to 580–940 amino acids of α-adaptin (Gonzalez-Gaitan and Jackle 1997) or that corresponding to 507–914 amino acids of β_2-adaptin were expressed in bacteria as His-tag and purified on Ni-NTA beads. The purified protein was injected into rabbits to generate antibodies (Deshpande Laboratories, Bhopal, India). These antibodies were affinity purified and used at 1:100 dilutions. For labeling the NMJs, third instar larvae were dissected in Ca^{2+}-free HL3 and fixed in 4% paraformaldehyde for 30 min. The fillets were washed in PBS containing 0.2% Triton X-100. The following primary antibodies were used for labeling the NMJs: mouse anti-CSP, 1:200 (Zinsmaier *et al.* 1994); rabbit anti-α-adaptin, 1:100, generated against the same region, as described previously (Gonzalez-Gaitan and Jackle 1997); rabbit anti-β_2-adaptin, 1:100 (this study) rabbit anti-Nwk (gift from Barry Ganetzky); mouse anti-Futsch, 1:50 (Roos *et al.* 2000), rabbit anti-Endophilin 1, 1:200 (Rikhy *et al.* 2002); rabbit anti-Dynamin 1, 1:200 (Estes *et al.* 1996); rabbit anti-Dap160, 1:400 (Roos and Kelly 1998); guinea-pig anti-Eps15, 1:200 (Koh *et al.* 2007); and rabbit anti-pMAD, 1:1000 (Persson *et al.* 1998), and HRP conjugated to FITC or Rhodamine, secondary antibodies conjugated to Alexa-488/568, and anti-GFP conjugated to Alexa-488 (Molecular Probes, Life Technologies) were used at 1:400. Images were captured with a Zeiss LSM780 confocal microscope and processed using Adobe Photoshop software. The synaptic fluorescence intensity of the various neuronal markers in the control, mutant, and rescue animals was quantified by capturing the images using the same parameters and settings. The average fluorescence intensity around individual boutons was calculated using the ImageJ software (ImageJ, National Institutes of Health). At least 50 boutons from four animals of each genotype were used for fluorescence intensity quantification. An identical area was selected in the background, and the intensity value was subtracted from the individual values. Statistical analysis was carried out using GraphPad Prism software (GraphPad Software, San Diego).

Western blotting

Third instar larval brains of control, mutant, and rescued animals were dissected out and homogenized in buffer containing 2% SDS (50 mM Tris-HCl, pH 6.8, 25 mM KCl, 2 mM EDTA, 0.3 M sucrose, and 2% SDS) at 75° in a water bath (Ruiz-Canada *et al.* 2004). The samples were further centrifuged at 4000 × *g*. The protein concentration was calculated using bicinchoninic acid (BCA) assay, and then lysates were boiled in 2× Laemmli buffer. Then 50 μg of protein of each genotype was separated on 10% SDS-PAGE and then transferred to Hybond-LFP PVDF membrane (Amersham, GE Healthcare Life Sciences). The membrane

was blocked with 5% fat-free milk for 1 hr at room temperature and then incubated with primary antibody at 4° overnight followed by 1 hr of incubation with HRP-conjugated secondary antibody at 1:20,000 dilution. Visualization of signals was accomplished by using the ECL-Plus detection system (Amersham, GE Healthcare Life Sciences) based on the standard protocol. Primary antibodies against the following proteins and dilutions were used: α-adaptin, 1:4000; β_2-adaptin, 1:4000; Dap160, 1:5000; Endophilin 1, 1:10,000; Dynamin 1, 1:10,000; Nwk, 1:10,000; Eps15, 1:3000; and α-actin, 1:5000. The synaptic level of clathrin was assessed using anti-GFP antibody at 1:5000.

FM1-43 dye uptake

FM1-43 dye uptake experiments were performed as described previously (Ramaswami *et al.* 1994). Briefly, larvae were dissected on Sylgard plates in HL3 medium and then incubated for 3 min in HL3 containing 90 mM KCl and 4 μM FM1-43. For endo-exo cycling pool (ECP) estimation, nerves innervating muscles six and seven were stimulated at 3 Hz for 3 min in HL3 buffer containing 1.5 mM Ca^{2+} and 4 μM FM1-43. For estimating ECP, 4 min after cessation of high-frequency stimulation, HL3 buffer was replaced with HL3 containing 1.5 mM Ca^{2+} and 4 μM FM1-43, and the nerve was again stimulated at 3 Hz for 3 min. The fillets were quickly washed five times with Ca^{2+}-free HL3 to remove excess dye. Preparations were imaged under a 63× water immersion objective lens using a QuantEM 512SC EMCCD camera (Photometrics, Tucson, AZ) mounted on an upright Axio Examiner D1 microscope with AxioVision software (Carl Zeiss). The average synaptic FM1-43 fluorescence was quantified using ImageJ.

SynaptopHluorin Imaging

SynaptopHluorin imaging was done using a Zeiss Axio Examiner D1 with a 63× 0.9-NA water immersion objective as described previously (Kumar *et al.* 2009). Briefly, third instar larvae were dissected in Ca^{2+}-free HL3; the buffer was later exchanged with 2.0 mM Ca^{2+} containing HL3 for imaging. Time-series imaging was performed by continuous exposure of 200 msec and intervals of 500 msec. Images were acquired using a cooled Evolve 512 Delta 512b EMCCD camera (Roper Scientific). The change in fluorescence ($\Delta F/F$) was calculated at each time point by defining a region of interest (ROI) that included at least 30 boutons from five different animals. The fluorescence intensity of the particular ROI at each time point after the stimulus was subtracted from the average fluorescence before stimulus. The tau (τ) value for SpH kinetics was calculated using GraphPad PRISM 5.01 by fitting the fluorescence decay curve after stimulus to one phase exponential.

Electrophysiology

Intracellular recordings were made from muscle 6 of the A2 hemisegment using sharp glass microelectrodes having resistance between 12 and 20 MΩ, and the technique has been described previously (Rikhy *et al.* 2002; Verstreken *et al.* 2002). All recordings were performed in HL3 containing 1.5 mM Ca^{2+}. Spontaneous release events were recorded for 60 sec. Nerves were stimulated at 1 Hz to record evoked junction potential (EJP). For synaptic depression experiments, nerves were stimulated at 10 Hz in 1.5 mM Ca^{2+} for 5 min. For recovery experiments, the larvae were stimulated at 10 Hz for 5 min followed by 90 sec of rest, and then test stimuli were given every 30 sec. Only muscles whose resting membrane potential was between −60 and −75 mV were used for recording. The quantal content was calculated by dividing average EJP amplitude by average miniature EJP (mEJP) amplitude for each NMJ. The signal was amplified using an Axoclamp 900A amplifier, and the data were acquired using a Digidata 1440A data-acquisition system and pClamp10 software (Axon Instruments). For data analysis, an offline software minianalysis (Synaptosoft) was used.

Intracellular recordings at 34° were performed at muscles 6/7 of the A2 hemisegment using sharp microelectrodes with 20- to 30-MΩ resistance, as described previously (Delgado *et al.* 2000). Briefly, wandering third instar larvae were dissected in 1.5 mM Ca^{2+} containing HL3 maintained at 30°. During recordings, temperature was maintained at 34° using a QE-1HC quick-exchange heated/cooled platform combined with a CL-100 bipolar temperature controller and a TCM-1 thermal cooling module (Warner Instruments).

Estimation of vesicle pool size

Third instar wandering larvae were dissected in Ca^{2+}-free HL3. Intracellular recordings were made from ventral longitudinal muscles 6/7 of the A2 abdominal hemisegment using sharp microelectrodes with 40–60 MΩ of resistance filled with a 1:1 mixture of 3M KAc and 3M KCl. For calculating ECP, the synapses were incubated in HL3 containing 1.0 mM of Ca^{2+} and 1.0 μM of Bafilomycin A1 for 15 min at room temperature. mEJPs were recorded for 60 sec, followed by continuous stimulation of synapses at 3 Hz until depletion in EJPs was detected. Quantal content was calculated by dividing the average EJP amplitude of each recording by the average mEJP amplitude. In order to calculate the cycling vesicle pool, the cumulative plot of quanta released over stimulus number was plotted, and linear regression to stimuli number 3800–6000 was exerted. ECP was measured from the *Y*-intercept of regression, calculated by back-extrapolating from stimuli number 3800–6000 (Kim *et al.* 2009). To obtain the total vesicle pool, the synapses were continuously stimulated at 10 Hz after recording spontaneous events in the presence of 1 μM Bafilomycin A1. The total vesicle pool was estimated by integrating quantal content over stimuli number in a synaptic depression plot until depletion was achieved (Delgado *et al.* 2000; Kim *et al.* 2009). Recordings in which a change in *V*m was <20% were used for analysis. Data were acquired using pClamp 10, and analysis was done in Clampfit 10 software.

22C10 loop quantification

Third instar larval fillets were double stained with HRP and 22C10, and images were captured using a Zeiss LSM780 confocal microscope with a 40× objective. Only NMJs of

muscles 6/7 of hemisegment A2 were used, and ImageJ was used for quantification. The image was digitally magnified, and the total number of boutons was first determined by manually counting the number of HRP-positive varicosities. This was followed by counting the number of complete looped structures that co-localized with HRP. Incomplete loops and loops with diffused or interrupted staining were not included in the count. It is to be noted that in the case of mutants, the faintly stained terminal loops were included in the count. The total number of loops was divided by the total bouton number to arrive at the percentage of boutons with loops (Roos *et al.* 2000).

Data availability

Antibodies and Drosophila lines generated and used in this manuscript will be made available upon request. Supplemental data is available as Figure S1, Figure S2, Figure S3, Table S1 and Table S2.

Results

angur is an allele of σ_2-adaptin, the smallest subunit of the AP2 complex

Three alleles of *angur* were obtained as second-site mutations through Δ2–3-mediated *P*-element mobilization of BL17200 and BL14472. All the heteroallelic mutant animals died at the third instar larval stage. The NMJ synapse in the mutants showed aberrant morphology resembling a bunch of grapes. Hence we named these mutants *angur* (a Hindi word meaning "bunch of grapes"). While $angur^{7}$ and $angur^{2}$ were obtained through *P*-element mobilization of $Synd^{EP877}$/TM6 (BL17200) located 2416 bp upstream of the Syndapin ORF, $angur^{5}$ was obtained independently through *P*-element mobilization of KG06118b (BL14472) located 406,920 bp downstream of the Syndapin ORF. Complementation analysis of these mutants showed that they belonged to the same complementation group. To ascertain the affected gene, we performed mapping with various deficiency lines spanning chromosome arm *3R*. The deficiency lines BL9485, BL9487, and BL26529 (having chromosomal deletion between $93B_6$ and $93F_{14}$) failed to complement the *angur* alleles (Figure 1A). We further checked for complementation of *angur* alleles with smaller deficiencies and mutations in this region. Interestingly, one of these mutant lines, BL13478 ($AP2\sigma^{KG02457}$), which is a *P*-element insertion in the third exon of the σ_2-adaptin ORF (Figure 1B), did not complement the *angur* alleles. To find the new genomic position of the *P*-elements in *angur* alleles, we performed plasmid rescue followed by sequencing. $angur^{2}$ and $angur^{7}$ were found to be present 147 and 153 bp upstream of a non-protein-coding gene, *Heat shock RNA omega* (*Hsrω*), respectively. Also, $angur^{5}$ was found to be present 136 bp upstream of *Hsrω*. Semiquantitative RT-PCR from these animals, however, showed the *Hsrω* transcript to be comparable to controls (Figure S1).

Surprisingly, sequencing of the σ_2-adaptin genomic region in *angur* alleles revealed that the ORF was intact. However, RT-qPCR analysis showed a severe reduction in the σ_2-adaptin transcript level in all the heteroallelic mutants or when σ_2-adaptin was ubiquitously knocked down using an RNAi (Figure 1C). Furthermore, both the lethality and the NMJ morphological defects could be rescued by ubiquitous expression of the σ_2-adaptin ORF in heteroallelic as well as $AP2\sigma^{KG02457}$ homozygous mutant animals (Figure 1D). Pan-neuronal expression of the σ_2-adaptin ORF using $elav^{C155}$-Gal4 in *angur* heterozygous mutants ($angur^{7}/AP2\sigma^{KG02457}$ or $angur^{7}/angur^{5}$) or in $AP2\sigma^{KG02457}$ homozygous mutants could rescue the synaptic phenotype but not the lethality. Thus, the upstream genomic region of *Hsrω* appears to contain regulatory sequences that control the expression of σ_2-adaptin. To assess whether the *P*-element insertions upstream of *Hsrω* affected the expression of other genes in this region, we performed RT-qPCR (data not shown) as well as semiquantitative RT-PCR and analyzed the expression of ETHR, SIFaR, Rab1, and CG5919, the genes flanking σ_2-adaptin. We did not detect any change in the expression of these genes, suggesting that the *P*-element insertions specifically disrupted σ_2-adaptin expression (Figure S1). Conversely, we also assessed whether synaptic morphology was altered in two of the *Hsrω* alleles that have been reported previously to affect *Hsrω* transcript levels, $Hsr\omega^{66}$ (~1.6 kb deletion in the *Hsrω* promoter region and the first nine bases of the first exon) and *EP93D* (an EP insertion upstream of *Hsrω*) (Sengupta and Lakhotia 2006; Lakhotia *et al.* 2012). We found that the synaptic morphology in these larvae was comparable to that in controls, and the σ_2-adaptin levels were unaltered (Figure S1), as assessed by α-adaptin staining. To avoid potential complications of the *P*-element insertions near the *Hsrω* locus, we also analyzed the allelic combinations of $AP2\sigma^{KG02457}$ with two of the deficiency lines, Df(3R)ED10838 and Df(3R)ED10845. These larvae showed similar synaptic phenotypes and severely reduced synaptic α-adaptin levels as $AP2\sigma^{KG02457}$ homozygous larvae or $AP2\sigma^{KG02457}/angur^{7}$ heteroallelic mutants (Figure S1). All these data suggest that *angur* is an allele of σ_2-adaptin and that the lethality and synaptic phenotype are due to the specific loss of σ_2-adaptin.

Mitotic clones of angur show a defect in eye morphology

Because *angur* mutants are homozygous lethal, we made mutant eye clones using the *eyFLP* system (Stowers and Schwarz 1999; Rikhy *et al.* 2002). The homozygous *angur* mutant eyes (*EGUF/+*; FRT82B, $angur^{7}$/FRT82B, GMR-*hid*) showed severe morphological defects with roughening and loss of bristles. The mutant eyes were also smaller than control eyes (Figure 2, A and B). Scanning electron microscopy revealed severely disorganized ommatidia of uneven size. Bristles were sparsely present in the mutant clones compared to the evenly spaced bristles in control eyes (FRT82B, $angur^{7}$) (Figure 2, D and E). The morphological defects and eye size

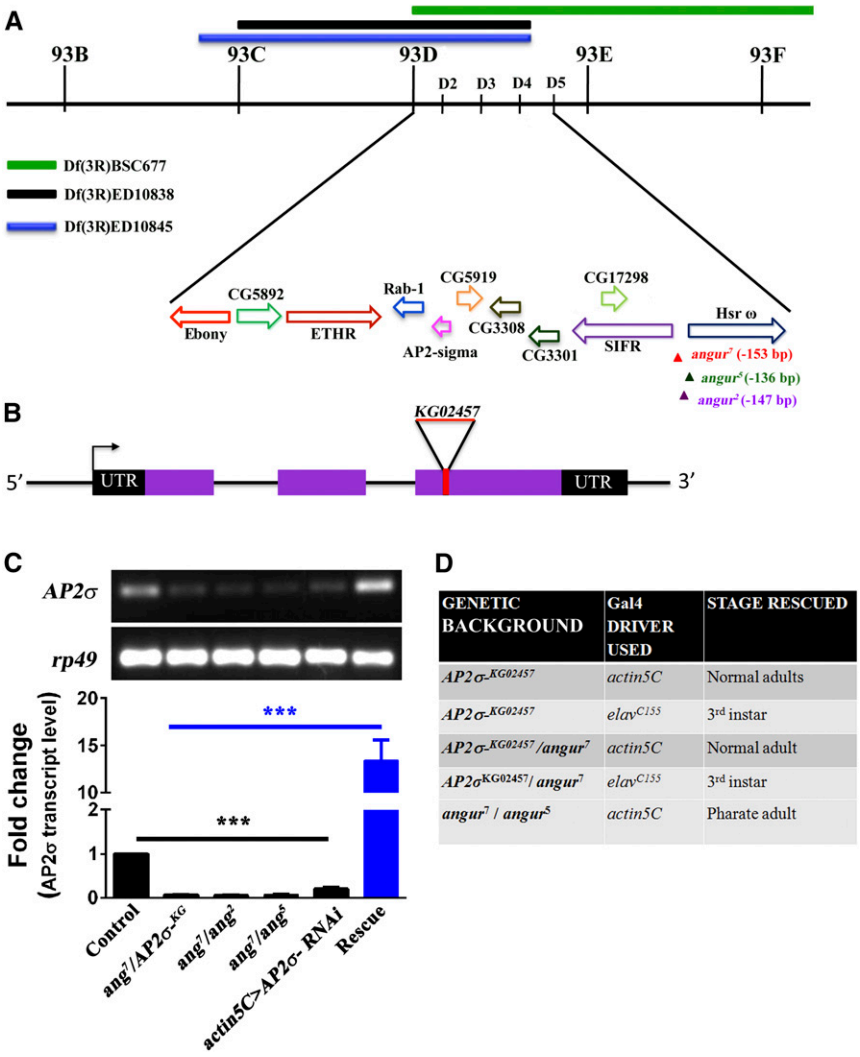

D

GENETIC BACKGROUND	Gal4 DRIVER USED	STAGE RESCUED
$AP2\sigma^{-KG02457}$	*actin5C*	Normal adults
$AP2\sigma^{-KG02457}$	$elav^{C155}$	3rd instar
$AP2\sigma^{-KG02457}/angur^{7}$	*actin5C*	Normal adult
$AP2\sigma^{KG02457}/angur^{7}$	$elav^{C155}$	3rd instar
$angur^{7}$ / $angur^{5}$	*actin5C*	Pharate adult

Figure 1 *angur* is an allele of σ_2-adaptin, the smallest subunit of adapter protein 2 (AP2) complex. (A) Deficiency mapping showed the *angur* locus to be located in the region of $93D_1$–$93D_4$ on the third chromosome of *Drosophila*. The three deficiency lines that uncovered the *angur* locus—Df(3R)BSC677, Df(3R)ED10838, and Df(3R)ED10845—are labeled. Solid bars mark the deleted regions in these deficiency lines. The $93D_1$–$93D_4$ region of the chromosome contains at least 10 identified genes. Different colored arrows represent the relative positions and orientations of the genes in the $93D_1$–$93D_4$ region. While $angur^7$ and $angur^2$ were obtained from mobilization of EP0877, $angur^5$ was obtained from mobilization of KG06118b. The *P*-element in *angur* alleles was located in the 5′ end of the *hsrω* gene but did not affect expression of the *hsrω* gene. (B) Genomic organization of the σ_2-adaptin locus showing exons (represented by solid boxes) and introns (represented by thin lines). The transcription start site is represented by an arrow, and the untranslated regions are shown by black solid boxes. The insertion site of *P*-element *KG02457* lies in the third exon of the gene. (C) Semi-quantitative (top panel) and quantitative RT-PCR (bottom panel) depicting transcript levels of σ_2-adaptin in controls, $angur^7/AP2\sigma^{KG02457}$, $angur^7/angur^2$, $angur^7/angur^5$, *actin5C*-Gal4-driven σ_2-adaptin RNAi, and rescued heteroallelic mutant (*actin5C*/+; $angur^7$/UAS-AP2σ, $AP2\sigma^{KG02457}$), respectively. σ_2-adaptin transcript level is dramatically reduced in the heteroallelic mutants or *actin5C*-Gal4-driven σ_2-adaptin RNAi. rp49 transcript level was used as an internal concentration control for messenger RNA (mRNA). The error bars in the bottom panel represent SEM. Statistical analysis based on one-way ANOVA followed by *post-hoc* Tukey's multiple comparison test. (D) Rescue of $AP2\sigma^{KG02457}$ mutants and heteroallelic combinations in homozygous or transheterozygous combinations using ubiquitous *actin5C*-Gal4 or the neuronal $elav^{C155}$-Gal4 drivers.

could be partly restored by expressing the σ_2-adaptin transgene in the mutant eyes (*EGUF/+*; FRT82B, $angur^7$, UAS-AP2σ/FRT82B, GMR-*hid*) (Figure 2, C and F). To delve into the ultrastructural defects, we performed TEM on these genotypes. The photoreceptor cells R1–R7 could be distinctly visualized in control eyes (Figure 2G). Interestingly, the homozygous mutant eye clones lacked the photoreceptor cells (Figure 2H), and this could be restored in the rescued animals (Figure 2I). We counted the number of photoreceptors in all genotypes from four different cartridges and found that it was always seven in control and rescue animals. In the mutant clones, however, we could not see any photoreceptor cells. Because photoreceptor cells were absent in the mutant clones, we hypothesized that synaptic transmission must be affected in them. To test this, we recorded ERGs and found that *angur* mutant eye clones showed minimal depolarization, suggesting that they failed to perceive light (Figure 2J). The eye morphology and ERG defects were partially restored by expressing the σ_2-adaptin transgene in the eyes. Rescue of the ERG defect was significant compared to the mutant ($P = 0.006$) (Figure 2K). Taken together, these data suggest that σ_2-adaptin-dependent endocytosis plays a crucial role in the biogenesis of rhabdomeres.

Subunits of AP2 are required for normal synapse morphology

The AP2 complex is believed to be essential for CME, and a block in the process results in defects in synaptic transmission (Gonzalez-Gaitan and Jackle 1997; Gu *et al.* 2013). Similarly, defects in the CME pathway due to mutations in proteins implicated in the pathway also lead to morphological defects at the *Drosophila* NMJs (Rikhy *et al.* 2002; Verstreken *et al.* 2002; Song and Zinsmaier 2003; Dickman *et al.* 2006). Our observations revealed severe structural defects (Figure 3, A–C) in *σ_2-adaptin* mutants suggesting that σ_2-adaptin-dependent endocytosis plays a crucial role in synaptic development. We observed that boutons

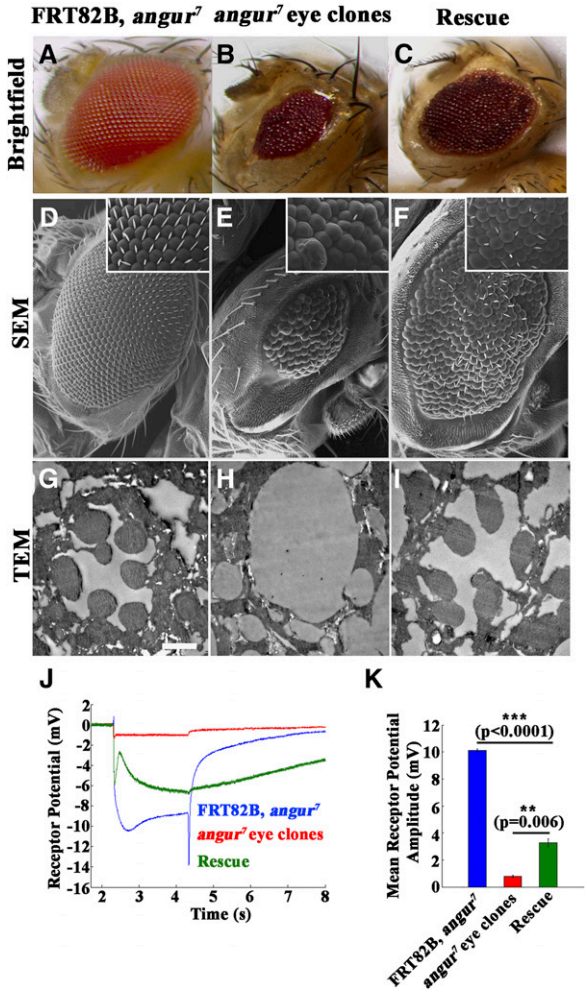

Figure 2 *angur* mutant eye clones show severe defects in rhabdomere development. (A–C) Brightfield images of (A) control (FRT82B, *angur*^{7}), (B) mutant *angur*^{7} eye clone (*EGUF*/+; FRT82B, *angur*^{7}/FRT82B, GMR-*hid*), and (C) transgene-rescued animal (*EGUF*/+; FRT82B, *angur*^{7}, UAS-AP2σ/FRT82B, GMR-*hid*). (D–F) SEMs of (D) control (FRT82B, *angur*^{7}), (E) mutant *angur*^{7} eye clone (*EGUF*/+; FRT82B, *angur*^{7}/FRT82B, GMR-*hid*), and (F) transgene-rescued animal (*EGUF*/+; FRT82B, *angur*^{7}, UAS-AP2σ/FRT82B, GMR-*hid*). (G–I) TEMs of (G) control (FRT82B, *angur*^{7}), (H) mutant *angur*^{7} eye clone (*EGUF*/+; FRT82B, *angur*^{7}/FRT82B, GMR-*hid*), and (I) transgene-rescued animal (*EGUF*/+; FRT82B, *angur*^{7}, UAS-AP2σ/FRT82B, GMR-*hid*). Scale bar, 2 μm. (J) ERG traces of control animals (FRT82B, *angur*^{7}) shown in blue, mutant *angur*^{7} eye clone animals (*EGUF*/+; FRT82B, *angur*^{7}/FRT82B, GMR-*hid*) shown in red, and transgene-rescued animal (*EGUF*/+; FRT82B, *angur*^{7}, UAS-AP2σ/FRT82B, GMR-*hid*) shown in green. (K) Histogram showing quantification of receptor potential amplitudes of the preceding genotypes. ***$P < 0.0001$. Error bars represent standard error of the mean. Statistical analysis based on one-way ANOVA followed by *post-hoc* Tukey's multiple-comparison test. Note that compared to the mutant eye clones, the rescued animals showed mild but significant rescue of receptor potential depolarization.

in σ_2-*adaptin* mutants were clustered in contrast to controls, where they are uniformly spaced. The σ_2-*adaptin* mutants showed an over twofold increase in the number of boutons (Figure 3K) (control: 98 ± 4.8; *angur*^{7}/*AP2σ*^{KG02457}: 185 ± 5.9; *angur*^{7}/*angur*^{5}: 274 ± 8.6), while there was a significant decrease in the bouton area (Figure 3L) (control: 8.7 ± 0.5 μm^2; *angur*^{7}/*AP2σ*^{KG02457}: 2.3 ± 0.13 μm^2; *angur*^{7}/*angur*^{5}: 2.5 ± 0.1 μm^2). Both lethality and morphological defects were rescued by ubiquitously expressing a σ_2-adaptin transgene in homozygous *AP2σ*^{KG02457} or heteroallelic σ_2-*adaptin* mutants using the *actin5C*-Gal4 driver (Figure 3D). Synaptic morphology defects but not lethality also could be rescued by expressing a σ_2-adaptin transgene using pan-neuronal drivers *elav*^{C155}-Gal4 or *nSyb*-Gal4, supporting the idea that morphological defects are due to a selective lack of σ_2-adaptin in neurons (Figure 1D). Average number of boutons reverted to wild-type levels in mutant animals rescued with a σ_2-adaptin transgene (*actin5C*/+; *angur*^{7}/*AP2σ*^{KG02457}, UAS-AP2σ: 89.88 ± 4.06). Similarly, the average size of an individual bouton also was restored to wild-type values in the rescued animals (*actin5C*/+; *angur*^{7}/*AP2σ*^{KG02457}, UAS-AP2σ: 6.38 ± 0.42 μm^2).

To analyze the consequence of loss of other subunits of the AP2 complex, we next asked whether reducing other components of AP2 would result into similar morphological defects. Predictably, we observed that RNAi-mediated knockdown of any of the subunits of AP2 with various tissue-specific Gal4 drivers yielded a wide range of phenotypes (Table S1). Importantly, knocking down any of the subunits of the AP2 complex in neurons phenocopied the σ_2-adaptin mutation (Figure 3, E–I and M, and Figure S2). Consistent with this observation, disrupting AP2 complex assembly in neurons by RNAi-mediated knockdown of phosphatidylinositol-4-kinase IIIα (PI4KIIIα), an enzyme that mediates the synthesis of PI(4)P, a precursor for biosynthesis of PI(4,5)P2, affected synapse morphology similar to other subunits of the AP2 complex (Figure 3J). The synaptic α-adaptin staining and the β_2-adaptin staining (not shown) were significantly reduced when the AP2 subunit or PI4KIIIα was neuronally knocked down (Figure S2). Taken together, these data suggest that all the subunits of AP2 along with phospholipid PI(4,5)P2 are obligate partners for regulating morphological plasticity at *Drosophila* NMJs.

σ$_2$-adaptin facilitates basal synaptic transmission

The AP2 complex is believed to be the major adapter for clathrin assembly during CME at the synapses and hence is believed to be essential for SV retrieval and regeneration of SVs for subsequent rounds of neurotransmitter release (Gonzalez-Gaitan and Jackle 1997; Collins *et al.* 2002; Heerssen *et al.* 2008; Cheung *et al.* 2010; Gu *et al.* 2013; Watanabe *et al.* 2014). Hence, in order to assess the need for the AP2 complex in endocytosis, we loaded σ_2-*adaptin* mutant and control synaptic terminals with FM1-43. Surprisingly, we found that dye uptake in *angur*^{7}/*AP2σ*^{KG02457}was reduced only by ~30% compared to control synapses (Figure 4, A and B) (compared to controls, FM1-43 fluorescence intensity in *angur*^{7}/*AP2σ*^{KG02457} was 72.03 ± 2.2%; *angur*^{7}/*angur*^{5} was 49.73 ± 1.6%; and *actin5C*/+; *angur*^{7}/*AP2σ*^{KG02457}, UAS-AP2σ was 82.08 ± 2.6%). Next, to ascertain the functional importance of σ_2-adaptin in synaptic transmission, we performed intracellular recordings at the NMJ of third instar larvae from σ_2-*adaptin* mutants. We observed that both mEJP amplitude

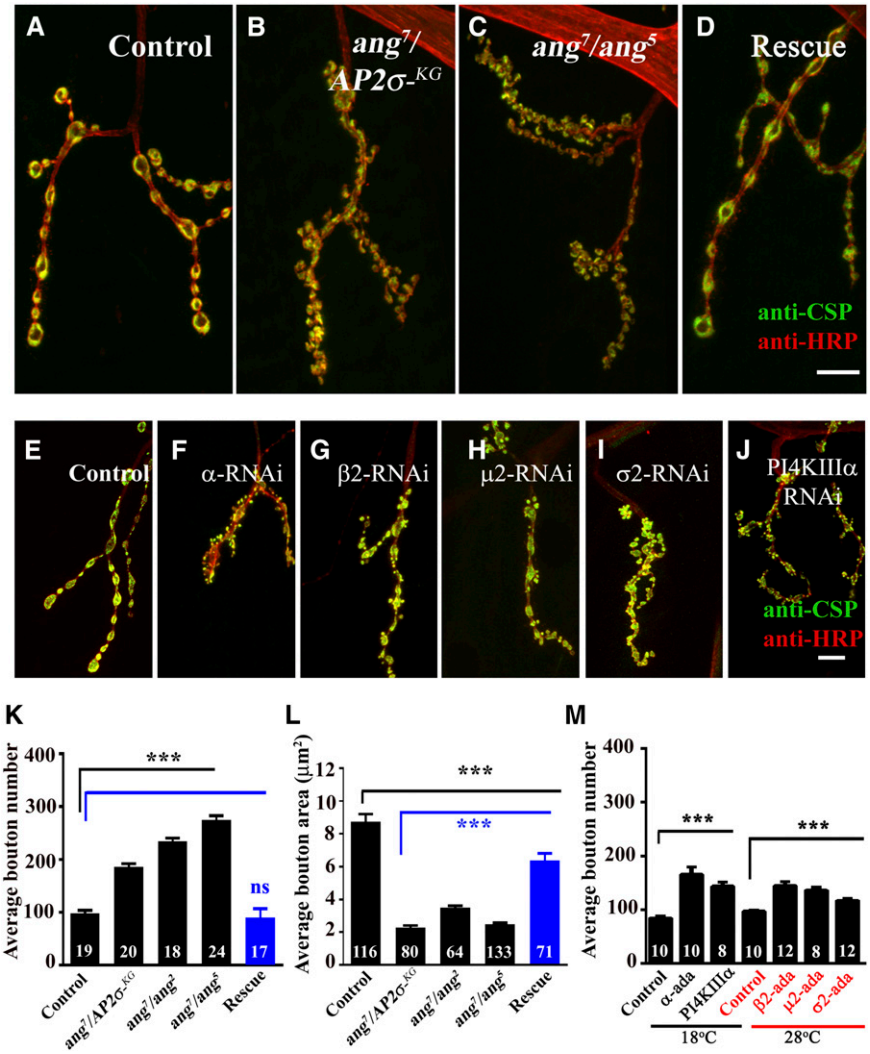

Figure 3 Mutation in σ_2-adaptin causes aberrant neuromuscular junction formation. (A–D) Confocal image of NMJ synapses at muscle 4 of (A) control animals, (B and C) heteroallelic *σ_2-adaptin* mutants (*angur^7/AP2σ^{KG02457}* and *angur^7/angur^5*), and (D) transgene-rescued animal (*actin5C/+*; *angur^7/UAS-AP2σ*, *AP2σ^{KG02457}*) double immunolabeled with a presynaptic marker CSP (green) and neuronal membrane marker HRP (red) to reveal the bouton outline. Compared to the control NMJ, the heteroallelic combination of *σ_2-adaptin* shows severely altered NMJ morphology. Scale bar, 15 μm. (E–J) Confocal images of NMJ synapses at muscle 4 co-labeled with CSP (green) and HRP (red) of (E) control and (F–J) neuronally expressing RNAi against AP2 complex subunits or PI4KIIIα: (F) *elav^{C155}/+*; α-adaptin RNAi/+, (G) *elav^{C155}/+*; β_2-adaptin RNAi/*UAS-Dicer*, (H) *elav^{C155}/+*; μ_2-adaptin RNAi/*UAS-Dicer*, (I) *elav^{C155}/+*; σ_2-adaptin RNAi/*UAS-Dicer*, and (J) *elav^{C155}/+*; PIK4IIIαRNAi/+. Note that neuronal knockdown of any of the subunits of the AP2 complex or PIK4IIIα phenocopies *σ_2-adaptin* mutations. Scale bar, 15 μm. (K) Histogram showing average number of boutons at muscles 6/7 of the A2 hemisegment in control animals (98.2 ± 4.8), heteroallelic *σ_2-adaptin* mutants (*angur^7/AP2σ^{KG02457}*: 185.4 ± 6; *angur^7/angur^2*: 233.4 ± 7; *angur^7/angur^5*: 274 ± 8.5) and the rescued animals (*actin5C/+*; *angur^7/UAS-AP2σ*, *AP2σ^{KG02457}*: 89.9 ± 4.0). The numbers in columns represent the number of 6/7 NMJs of the A2 segment used for bouton quantification. ***$P < 0.0001$. Error bars represent standard error of the mean. Statistical analysis based on one-way ANOVA followed by *post-hoc* Tukey's multiple-comparison test. (L) Histogram showing average bouton area in control animals (8.7 ± 0.5 μm^2), heteroallelic *σ_2-adaptin* mutants (*angur^7/AP2σ^{KG02457}*: 2.3 ± 0.13 μm^2; *angur^7/angur^2*: 3.5 ± 0.12 μm^2; *angur^7/angur^5*: 2.5 ± 0.1 μm^2) and rescued animals (*actin5C/+*; *angur^7/UAS-AP2σ*, *AP2σ^{KG02457}*: 6.4 ± 0.4 μm^2). The numbers in columns represent the number of boutons used for quantification. ***$P < 0.0001$. Error bars represent standard error of the mean. Statistical analysis based on one-way ANOVA followed by *post-hoc* Tukey's multiple-comparison test. (M) Histogram showing quantification of average bouton numbers at muscles 6/7 of the A2 hemisegments of third instar larvae in control animals and neuronally expressing RNAi against AP2 subunits (control at 18°, 85 ± 3; control at 28°, 98 ± 2; α-adaptin, 167 ± 13; β_2-adaptin, 145 ± 7.0; μ_2-adaptin, 137 ± 5; σ_2-adaptin, 118 ± 4) or PI4KIIIα (144 ± 7). At least 16 NMJ synapses of muscles 6/7 of the A2 hemisegment of each genotype were used for counting the number of boutons. ***$P < 0.0001$. The numbers in the columns represent the number of animals used for quantification. Error bars represent standard error of the mean. Statistical analysis based on one-way ANOVA followed by *post-hoc* Tukey's multiple-comparison test.

and frequency were significantly higher in *σ_2-adaptin* mutants compared to controls (Figure 4, C and E). However, EJP amplitude in *σ_2-adaptin* mutants was reduced compared to control synapses (control: 43.25 ± 1.7 mV; *angur^7/AP2σ^{KG02457}*: 31.60 ± 1.9 mV; *angur^7/angur^5*: 28.34 ± 1.1 mV) (Figure 4, D and F). Moreover, the quantal content in *σ_2-adaptin* mutants was significantly reduced (control: 67.63 ± 3.37; *angur^7/AP2σ^{KG02457}*: 35.48 ± 2.5; *angur^7/angur^5*: 34.54 ± 2.3) (Figure 4G). All the physiological characteristics were restored to normal levels when a σ_2-adaptin transgene was expressed in the mutant neurons (EJP amplitude in *actin5C/+*; *angur^7/AP2σ^{KG02457}*, UAS-AP2σ: 42.06 ± 1.1 mV; quantal content in *actin5C/+*; *angur^7/AP2σ^{KG02457}*, UAS-AP2σ: 64.54 ± 5.2). Consistent with this observation, reducing α-adaptin levels in neurons resulted in a similar reduction in EJP amplitude and quantal content (Figure 4, D, F, and G) (EJP amplitude in *elav^{C155}/+*; α-adaptin RNAi/+: 25.17 ± 2.2 mV; quantal content in *elav^{C155}/+*; α-adaptin RNAi/+: 27.26 ± 2.53). Taken together, these data suggest that σ_2-adaptin facilitates the basal synaptic transmission at *Drosophila* NMJ synapses.

The functional requirement of the AP2 complex in SV membrane retrieval at mammalian hippocampal synapses has been debated (Kononenko *et al.* 2014; Watanabe *et al.* 2014). Hence, in order to test the functional requirement of σ_2-adaptin in SV re-formation from the presynaptic membrane, we directly measured the rate of re-formation of normal-pH synaptic vesicles using synaptopHluorin imaging (Poskanzer *et al.* 2006; Kumar *et al.* 2009). Interestingly, we found that the kinetics of membrane retrieval

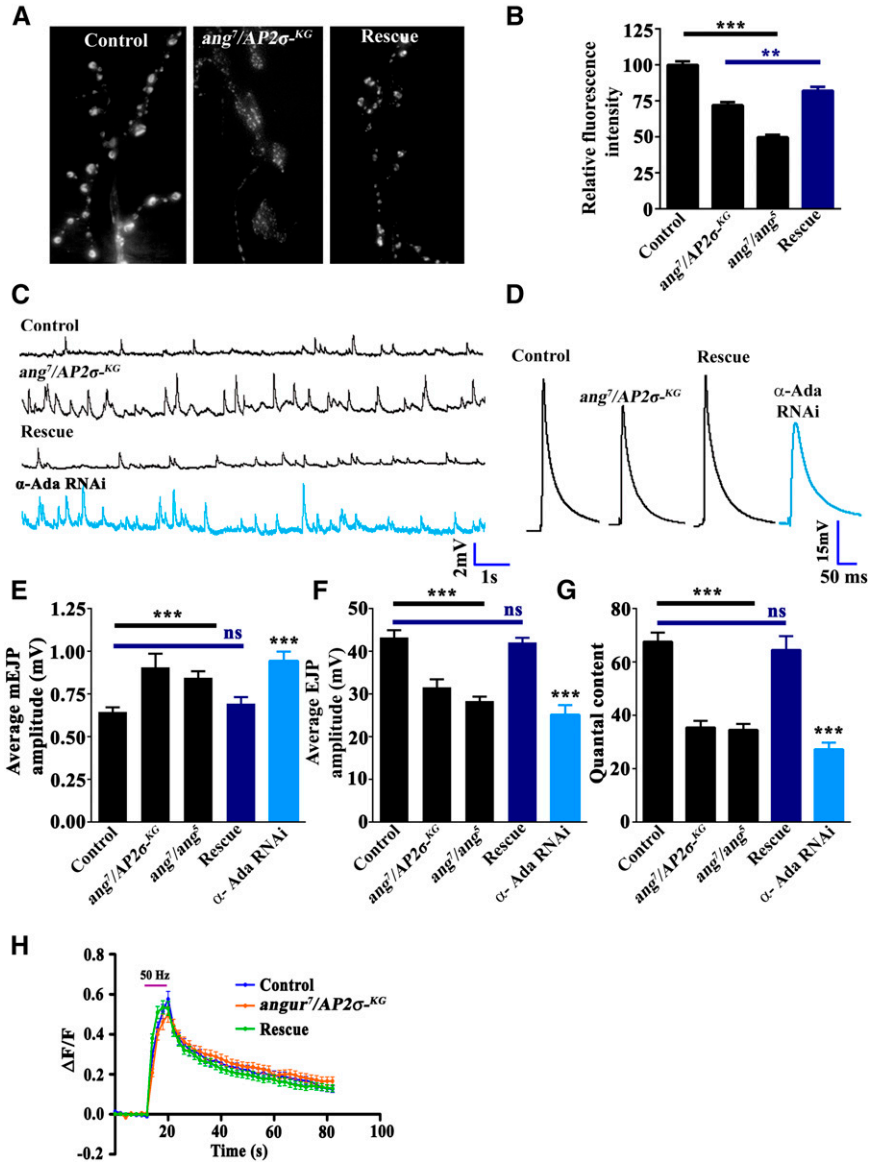

Figure 4 σ_2-adaptin facilitates basal synaptic transmission as well as synaptic vesicle endocytosis. (A) Representative images of FM1-43 dye uptake by control, heteroallelic *σ_2-adaptin* mutant (*angur^7/AP2$\sigma^{KG02457}$*), and transgene-rescued (*actin5C/+*; *angur^7/UAS-AP2σ*, *AP2$\sigma^{KG02457}$*) synapses. (B) Relative synaptic FM1-43 fluorescence uptake in control, heteroallelic *σ_2-adaptin* mutant (*angur^7/AP2$\sigma^{KG02457}$*: 72.1 ± 2.3% and *angur^7/angur^5*: 49.73 ± 1.7%) and transgene-rescued (*actin5C/+*; *angur^7/UAS-AP2σ*, *AP2$\sigma^{KG02457}$*: 82.1 ± 2.6%) synapses. ***$P < 0.0001$; **$P < 0.001$. Error bars represent standard error of the mean. Statistical analysis based on one-way ANOVA followed by *post-hoc* Tukey's multiple-comparison test. (C) Representative traces of mEJP in control animals, heteroallelic *σ_2-adaptin* mutant combinations (*angur^7/AP2$\sigma^{KG02457}$* and *angur^7/angur^5*), transgenic-rescued animals (*actin5C/+*; *angur^7/UAS-AP2σ*, *AP2$\sigma^{KG02457}$*), and *elav^{C155}/+*; α-adaptin RNAi/+ animals. (D) Representative traces of EJPs in control animals, *σ_2-adaptin* heteroallelic mutant combinations (*angur^7/AP2$\sigma^{KG02457}$* and *angur^7/angur^5*), transgene-rescued animals (*actin5C/+*; *angur^7/UAS-AP2σ*, *AP2$\sigma^{KG02457}$*), and *elav^{C155}/+*; α-adaptin RNAi/+ animals. (E) Histogram showing average mEJP amplitude in control animals (0.65 ± 0.03 mV), heteroallelic *σ_2-adaptin* mutants (*angur^7/AP2$\sigma^{KG02457}$*: 0.91 ± 0.08 mV; *angur^7/angur^5*: 0.85 ± 0.04 mV), transgene-rescued animals (*actin5C/+*; *angur^7/UAS-AP2σ*, *AP2$\sigma^{KG02457}$*: 0.69 ± 0.04 mV), and *elav^{C155}/+*; α-adaptin RNAi/+ (0.94 ± 0.06 mV) animals. At least 8 NMJ recordings of each genotype were used for quantification. ***$P < 0.0001$. Error bars represent standard error of the mean. Statistical analysis based on one-way ANOVA followed by *post-hoc* Tukey's multiple-comparison test. (F) Histogram showing average EJP amplitude in control animals (43.25 ± 1.67 mV), heteroallelic *σ_2-adaptin* mutants (*angur^7/AP2$\sigma^{KG02457}$*: 31.60 ± 1.9 mV; *angur^7/angur^5*: 28.34 ± 1.05 mV), transgene-rescued animals (*actin5C/+*; *angur^7/UAS-AP2σ*, *AP2$\sigma^{KG02457}$*: 42.06 ± 1.14 mV), and *elav^{C155}/+*; α-adaptin RNAi/+ (25.17 ± 2.24 mV) animals. At least 8 NMJ recordings of each genotype were used for quantification. ***$P < 0.0001$. Error bars represent standard error of the mean. Statistical analysis based on one-way ANOVA followed by *post-hoc* Tukey's multiple-comparison test. (G) Quantification of quantal content in control animals (67.63 ± 3.37), heteroallelic *σ_2-adaptin* mutants (*angur^7/AP2$\sigma^{KG02457}$*: 35.48 ± 2.45; *angur^7/angur^5*: 34.54 ± 2.25), transgene-rescued animals (*actin5C/+*; *angur^7/UAS-AP2σ*, *AP2$\sigma^{KG02457}$*: 64.54 ± 5.18), and *elav^{C155}/+*; α-adaptin RNAi/+ (27.26 ± 2.53) animals. ***$P < 0.0001$. Error bars represent standard error of the mean. Statistical analysis based on one-way ANOVA followed by *post-hoc* Tukey's multiple-comparison test. (H) Graph showing the SpH fluorescence response to a 50-Hz stimulus train for 10 sec in 2.0 mM Ca^{2+} containing HL3 of control (blue, $n = 37$ boutons, 5 animals; *elav^{3E1}*, *UAS-SpH/+*), mutant (orange, $n = 33$ boutons, 5 animals; *elav^{3E1}*, *UAS-SpH*, *AP2$\sigma^{KG02457}$/ang^7*), and rescued (green, $n = 29$ boutons, 5 animals; *elav^{3E1}*, *UAS-SpH*, *AP2$\sigma^{KG02457}$/ang^7*, *UAS-AP2σ*) synapses. The pink horizontal bar represents the stimulation time. Tau values were calculated after 10 sec of stimulation by fitting the fluorescence decay curve to one-phase exponential. *σ_2-adaptin* mutant (7.60 ± 0.17) shows a mild but significant difference in SpH kinetics compared to control (6.91 ± 0.17) and rescue (6.60 ± 0.23).

and acidification was mildly but significantly different in *σ_2-adaptin* mutants compared to control animals. The rates of re-formation of synaptic vesicles were $\tau = 6.9 \pm 0.17$ sec and $\tau = 7.6 \pm 0.17$ sec for control anmals and *σ_2-adaptin* mutants, respectively, when fit to a single exponential function (Figure 4H). Hence, taken together, our data suggest that the AP2 complex has a minimal role in SV retrieval from the presynaptic membrane at *Drosophila* NMJ synapses.

Compromised SV trafficking in *Drosophila* leads to synaptic fatigue at high-frequency nerve stimulation and also leads to temperature-dependent paralysis (Kosaka and Ikeda 1983; Zinsmaier *et al.* 1994; Rikhy *et al.* 2002; Verstreken *et al.* 2002; Koh *et al.* 2004). Hence, we tested whether reducing σ_2-adaptin levels leads to paralysis and synaptic fatigue at elevated temperature. Interestingly, we found that neuronal knockdown of σ_2-adaptin (*elav^{C155}/+*; σ_2-adaptin RNAi/+) results in temperature-dependent paralysis above

35° (Figure 5, A–C). We found that high-frequency nerve stimulation in *angur* mutants or in animals with neuronally reduced σ_2- or α-adaptin at 34° leads to an activity-dependent decline of EJP amplitude; however, unlike with *shibire^{ts}* alleles, the neurotransmitter release was not completely abolished (Figure 5, D–I). These data suggest that unlike essential endocytic proteins such as Endophilin and Shibire, AP2-modulated vesicle trafficking and its activity are also required during elevated temperatures to sustain neurotransmitter release.

σ_2-adaptin regulates synaptic vesicle regeneration under high-frequency nerve firing

To further assess a requirement for σ_2-adaptin in SV recycling, we stimulated the *σ_2-adaptin* mutant synapses in larval body wall muscle for 5 min at 10 Hz and recorded EJPs. While the control and rescued synapses (*actin5C/+*; *angur^7/AP2σ^{KG02457}*, UAS-AP2σ) did not show stimulation-dependent decline in EJP amplitudes over 5 min, mutant synapses (*angur^7/AP2σ^{KG02457}* and *angur^7/angur^5*) exhibited a significant decline in EJP amplitude (Figure 6, A and B). The decline in EJP amplitude at the end of 5 min of 10 Hz of nerve stimulation was ∼50% relative to the first stimulus. Similar results were obtained when α-adaptin was neuronally reduced (*elav^{C155}/+*; α-adaptin RNAi/+) (Figure 6, A and B). Thus, these data suggest that not only is AP2 required for maintaining basal synaptic transmission, but it is also crucial under high-frequency nerve firing to resupply SVs at *Drosophila* NMJ synapses.

Synaptic mutants implicated in CME, such as *endophilin* and *dap160*, show complete recovery from synaptic depression within a few minutes of rest after cessation of high-frequency stimulation, suggesting that synaptic membrane retrieval for vesicle regeneration in these mutants is stimulus dependent (Marie *et al.* 2004; Dickman *et al.* 2005). In contrast, we found that *σ_2-adaptin* mutants or animals with neuronally reduced α-adaptin do not recover from synaptic depression even after 4 min of rest following cessation of high-frequency stimulation. This observation suggests that in addition to its requirement in synaptic membrane retrieval, AP2 complex function is also required during the much slower process of SV trafficking, possibly at one of the rate-limiting steps in SV regeneration (Figure 6B). Hence, we reasoned that the mutants do not recover from synaptic depression because of compromised SV regeneration. To address this directly, we labeled larval NMJ synapses of control and mutant animals (*angur^7/AP2σ^{KG02457}* and *angur^7/angur^5*) with FM1-43 before or after 4 min of rest following cessation of high-frequency stimulation and estimated the ECP. Surprisingly, we found that even after 4 min of rest, the total recycling pool did not recover to its initial value in the mutants or at the synapses where α-adaptin was reduced in the neurons (*elav^{C155}/+*; α-adaptin RNAi/+) (Figure 6C). Taken together, these data uncover a role for AP2 in the regeneration of synaptic vesicles under high-frequency stimulation in *Drosophila*.

To further investigate the underlying mechanism of synaptic fatigue in *angur* mutants, we estimated ECP and the total vesicle pool at the NMJ synapses. In order to measure ECP, synapses were continuously stimulated in the presence of 1 μM Bafilomycin A1 at 3 Hz until synaptic depression was attained. The initial decline in quantal content during the short duration of neuronal activity or at 3 Hz stimulation mostly represents ECP; however, the later depletion reflects the mobilization of vesicles from the reserve pool (Kim *et al.* 2009). Consistent with our previous observations, the number of vesicles in ECP was found to be significantly lower in *angur* mutants (*angur^7/AP2σ^{KG02457}*: 16,590 ± 974; *angur^7/angur^5*: 15,040 ± 870; controls: 25,050 ± 1511). Similar results were obtained when α-adaptin levels were neuronally reduced (*elav^{C155}-GAL4 > α-adaptin RNAi*: 15,730 ± 1033; controls: 25,050 ± 1511) (Figure 6, D and E). The number of SVs in the ECP of rescued synapses (*actin5C-GAL4/+*; *angur^7/UAS-AP2σ*, *AP2σ^{KG02457}*: 23,635 ± 1358.75) was comparable to that in control animals (Figure 6, D and E). The total vesicle pool was measured by continuously stimulating the synapses at 10 Hz in the presence of 1 μM Bafilomycin A1. We quantified the total vesicle pool by integrating the quantal content from the depression curve (Figure 6F) until remarkable depletion was attained. Our data suggest significant reduction of the total vesicle pool in *angur* mutant (*angur^7/AP2σ^{KG02457}*: 53,220 ± 3156; *angur^7/angur^5*: 50,930 ± 2877) or neuronally reduced α-adaptin (*elav^{C155}-GAL4 > α-adaptin RNAi*: 63,460 ± 3650) synapses compared to control (94,610 ± 5929) and rescued synapses (*actin5C-GAL4/+*; *angur7/UAS-AP2σ*, *AP2σ^{KG02457}*: 102,200 ± 6315) (Figure 6G). Taken together, these data suggest that σ_2-adaptin is required to maintain the vesicle pool at *Drosophila* NMJ synapses. The synaptic depression observed under high-frequency stimulation is possibly due to less availability of SVs at the *σ_2-adaptin* mutant synapses.

σ_2-adaptin is an obligate member for stabilizing the AP2 complex and clathrin but not other synaptic proteins

Because the AP2 complex acts as a hub for several molecular interactions during CME, we next asked whether σ_2-adaptin affects localization or stability of other synaptic proteins (Schmid and McMahon 2007). To address this, we quantified the synaptic immunofluorescence levels of various synaptic proteins in *σ_2-adaptin* mutants. We observed a severe reduction in synaptic α-adaptin (compared to controls, the α-adaptin fluorescence intensity in *angur^7/AP2σ^{KG02457}* was 5.6 ± 0.2%; in *angur^7/angur^5* was 1.4 ± 0.1%, and in *actin5C/+*; *angur^7/AP2σ^{KG02457}*, UAS-AP2σ was 73.46 ± 1.6%), and β_2-adaptin immunoreactivity (compared to controls, the β_2-adaptin fluorescence intensity in *angur^7/AP2σ^{KG02457}* was 16.53 ± 1.4%; in *angur^7/angur^5* was 31.97 ± 1.6%; and in *actin5C/+*; *angur^7/AP2σ^{KG02457}*, UAS-AP2σ was 76.07 ± 2.0%) at the *σ_2-adaptin* mutant synapses (Figure 7, A and B). Because the AP2 complex is involved in clathrin recruitment, we speculated that the

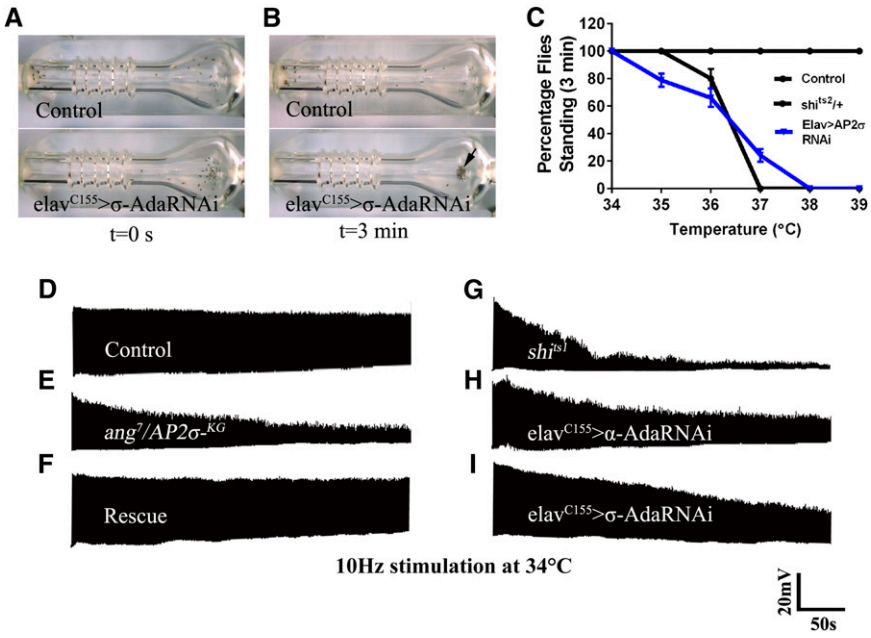

Figure 5 Reducing σ_2-adaptin levels in neurons causes temperature-sensitive paralysis at elevated temperature. (A and B) Control (*elav*^{C155}/+) 2- to 3-day-old adult flies do not suffer paralysis in 3 min at 38°, whereas similarly aged adult flies expressing σ_2-adaptin RNAi (*elav*^{C155}/+; σ_2-adaptin RNAi/+) in neurons showed complete paralysis in 3 min at 38°. These animals recovered within 2 min when shifted to 25° (not shown). (C) Paralysis profile of control animals and animals expressing RNAi against σ_2-adaptin in neurons (*elav*^{C155}/+; σ_2-adaptin RNAi/+) and *shi*^{ts2}/+. While the control animals do not suffer paralysis in 3 min, the RNAi-expressing animals are paralyzed above 35°. Five trials were performed for each genotype at each temperature in a sushi cooker (Ramaswami *et al.* 1993). Each trial contained 10–15 animals. Error bars represent standard error of the mean. (D–I) Representative traces of EJPs under high-frequency stimulation of indicated genotypes stimulated at 10 Hz for 5 min at 34° in 1.5 mM Ca^{2+} containing HL3. Unlike *shibire*^{ts1} (G), mutant (E) and neuronally reduced α- or σ_2- adaptin (H and I) animals do not show complete reduction in EJP amplitude at the end of 5 min of stimulation.

levels of clathrin at the mutant synapses might be altered. Hence, to assess the levels of clathrin at the *σ_2-adaptin* mutant synapses, we overexpressed an EYFP-tagged *Clc* transgene in neurons of heteroallelic *σ_2-adaptin* mutants (*elav*^{C155}/+; *UAS-Clc*/+; *angur*^{7}/*AP2σ*^{KG02457}) or in the rescue animals (*elav*^{C155}/+; *UAS-Clc*/+; *angur*^{7}/*AP2σ*^{KG02457}, *UAS-AP2σ*). Compared to controls (*elav*^{C155}/+; *UAS-Clc*/+), the EYFP fluorescence intensity at mutant (48.5 ± 2.3%) synapses was dramatically reduced but was significantly restored in the rescue (84.7 ± 4.1%) synapses (Figure 7C and Figure S3). Other synaptic proteins implicated in CME were not altered in *σ_2-adaptin* mutants (Figure 7, D and E, and Figure S3) Taken together, these data suggest that all the subunits of the AP2 complex are specifically essential for recruitment and/or stability of clathrin at the synapse.

The altered synaptic abundance of α-adaptin, β_2-adaptin, or clathrin in *σ_2-adaptin* mutants could be the result of either degradation of these proteins or a defect in synaptic targeting. To address this, we performed Western blots on lysates prepared from third instar larval brain. We observed a severe reduction in the α-adaptin, β_2-adaptin, and clathrin protein levels in *σ_2-adaptin* mutants (Figure 7F). Consistent with the immunofluorescence studies, the levels of other synaptic proteins, such as Endophilin1, Dynamin1, Dap160, Eps15, and Nwk, were not significantly altered in *σ_2-adaptin* mutants (Figure 7, D and E, and Figure S3). Hence, these data suggest that σ_2-adaptin is critically important for stabilizing not only the AP2 complex but also clathrin. Moreover, AP2 appears to be specific adapter for clathrin at the synapses of *Drosophila* NMJ.

Microtubule-based cytoskeleton is disorganized in σ_2-adaptin mutants

It has been shown that synaptic growth is controlled via regulation of the synaptic microtubule cytoskeleton and that any alteration of this cytoskeleton affects synaptic growth (Roos *et al.* 2000). To examine whether the microtubule cytoskeleton was disrupted in the mutant NMJ synapses, we labeled the synapses with MAb 22C10. This antibody labels Futsch, which is associated with the dendritic, axonal, and nerve-terminal cytoskeleton (Roos *et al.* 2000). In control boutons, the microtubules appeared continuous with periodic loop structures (Figure 8, A, B, and G) (24.75 ± 1.7% of type Ib boutons on muscles 6 and 7 of the A2 hemisegment). Contrary to the control boutons, the microtubules in the *σ_2-adaptin* mutant boutons appeared fragmented, with almost total disappearance of the periodic loop structures (Figure 8, C, D, and G) (*angur*^{7}/*AP2σ*^{KG02457}: 4.42 ± 0.6% and *angur*^{7}/*angur*^{5}: 3.33 ± 0.5% of type Ib boutons on muscles 6 and 7 of the A2 hemisegment). These periodic loop structures could be rescued by ubiquitous σ_2-adaptin transgene expression (Figure 8, E, F, and G) (*actin5C*/+; *angur*^{7}/*AP2σ*^{KG02457}, UAS-AP2σ: 24.98 ± 2.9% of type Ib boutons on muscles 6 and 7 of the A2 hemisegment). RNAi-mediated knockdown of any of the subunits of AP2 or PI4KIIIα in neurons also resulted in a significant decrease in the number of periodic loop structures (Figure S2). These data suggest that σ_2-adaptin regulates NMJ morphology by regulating the cytoskeletal architecture.

Because BMP signaling is required for a normal microtubule cytoskeleton (Wang *et al.* 2007), we assessed whether this signaling pathway was affected in *σ_2-adaptin* mutants. We estimated the synaptic levels of pMAD and found that the mutant synapses had over threefold higher levels of pMAD compared to controls (Figure 8, H and I) (compared to controls, the pMAD fluorescence intensity in *endo*$^{\Delta 4}$ was 332.5 ± 16.7%; *angur*^{7}/*AP2σ*^{KG02457} was 345.8 ± 12.6%; *angur*^{7}/*angur*^{5} was 362.8 ± 14.6%, and *actin5C*/+; *angur*^{7}/

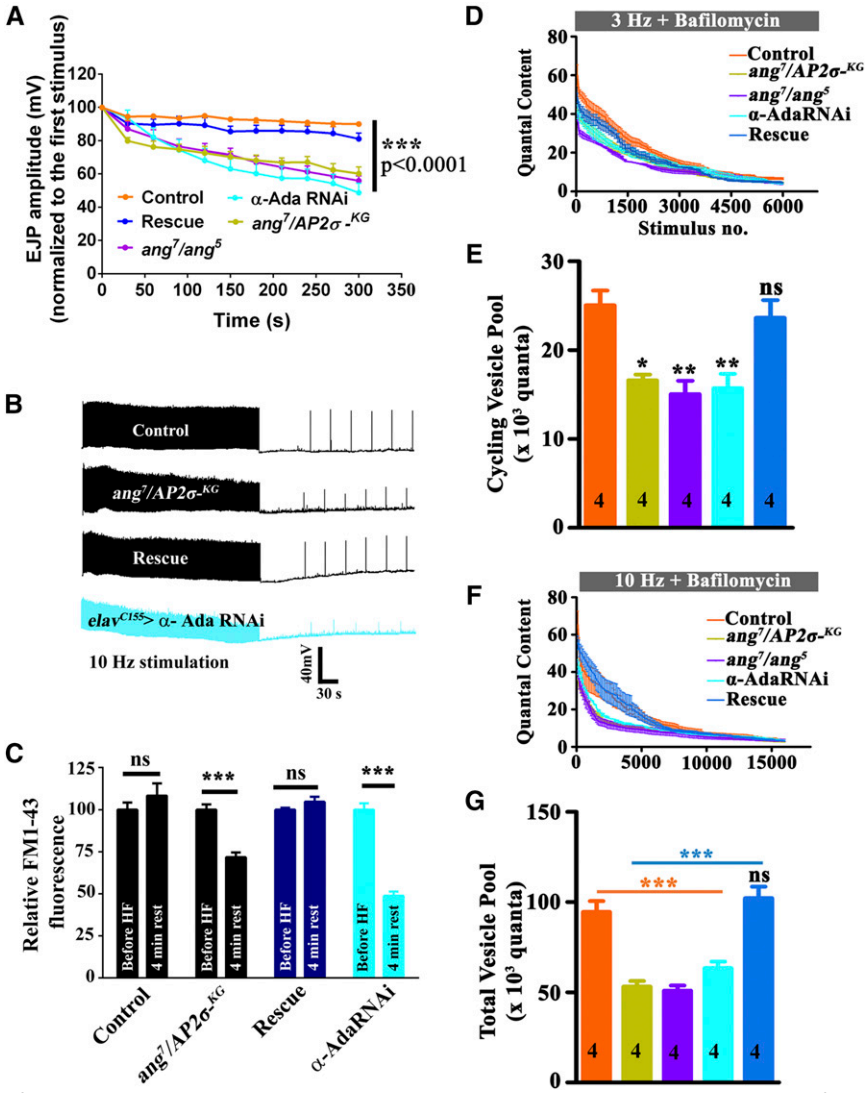

Figure 6 σ_2-adaptin function is essential under high-frequency stimulation to regenerate synaptic vesicles. (A) Normalized EJP amplitudes in control, heteroallelic *σ_2-adaptin* mutant (*angur^7/AP2σ^{KG02457}*and *angur^7/angur^5*), rescued larvae (*actin5C/+*; *angur^7/UAS-AP2σ*, *AP2σ^{KG02457}*), and neuronally knocked down α-adaptin (*elav^{C155}/+*; α-adaptin RNAi/+) animals stimulated at 10 Hz for 5 min in 1.5 mM Ca^{2+}. The mutant larvae showed stimulus-dependent decline in the EJP amplitudes over time. (B) Representative traces of indicated genotypes under high-frequency stimulation at 10 Hz for 5 min in 1.5 mM Ca^{2+} containing HL3. After 1.5 min of rest, test stimuli were given every 30 sec to assess the recovery of EJP from synaptic depression. Note that the mutant synapses do not recover to the first stimulus levels even after 4 min of rest from high-frequency stimulation. (C) Estimation of endo-exo cycling pool at NMJ synapses of indicated genotypes before high-frequency stimulation and after 4 min of rest from high-frequency stimulation. While the controls and rescue synapses maintained the ECP pool to its initial value after 4 min of rest, the *σ_2-adaptin* mutant synapses and the *elav^{C155}/+*; α-adaptin RNAi/+ synapses show significant decline in the endo-exo cycling pool and do not recover to the initial value after 4 min of rest. *n* = 50 boutons from eight different NMJs of muscles 6/7 of the A2 hemisegment were counted. (D) Synaptic depression curve showing the depletion in quantal content over stimulus number in synapses stimulated at 3 Hz in the presence of 1 μM Bafilomycin A1 to deplete ECP. (E) Histogram showing ECP estimates of control (25,050 ± 1511), heteroallelic mutants (*angur^7/AP2σ^{KG02457}*: 16,590 ± 974; *angur^7/angur^5*: 15,040 ± 870), *elav^{C155}/+*; α-adaptin RNAi/+ (15,730 ± 1031), and rescued animals (*actin5C-GAL4/+*; *angur^7/UAS-AP2σ*, *AP2σ^{KG02457}*: 23,635 ± 1358) obtained from *Y*-intercept of regression, calculated by back-extrapolating from stimulus numbers 3800–6000 on a cumulative plot of Figure 6D. $^{**}P \leq 0.0006$; $^{*}P \leq 0.0007$. Numbers in the columns represent the number of animals used for experiments and quantification. The error bars represent standard error of the mean. Statistical analysis based on one-way ANOVA followed by *post-hoc* Tukey's multiple-comparison test. (F) Synaptic depression curve showing the depletion of the total vesicle pool over stimulus number estimated by stimulating the synapses at 10 Hz in presence of 1 μM Bafilomycin A1. (G) Histogram showing the estimation of total vesicle pool of control animals (94,610 ± 5929), heteroallelic mutants (*angur^7/AP2σ^{KG02457}*: 53,220 ± 3156; *angur^7/angur^5*: 50,930 ± 2877), *elav^{C155}/+*; α-adaptin RNAi/+ (63,460 ± 3650), and the rescued animals (*actin5C-GAL4/+;angur^7/UAS-AP2σ*, *AP2σ^{KG02457}*: 102,200 ± 6315) calculated by integrating quantal content over stimulus number in synaptic depression plot of Figure 6F until depletion was achieved. $^{***}P < 0.0001$. Numbers in the columns represent the number of animals used for experiments and quantification. The error bars represent standard error of the mean. Statistical analysis based on one-way ANOVA followed by *post-hoc* Tukey's multiple-comparison test.

AP2σ^{KG02457}, UAS-AP2σ was 102.2 ± 5.1%). Because pMAD has been shown to accumulate in the motor nuclei of synaptic mutants, we analyzed nuclear pMAD levels in *σ_2-adaptin* mutants. Consistent with other endocytic mutants (Vanlandingham *et al.* 2013), we found significantly elevated pMAD levels in the motor nuclei of *σ_2-adaptin* mutants (*angur^7/AP2σ^{KG02457}*: 162.5 ± 5.6% and *angur^7/angur^5*: 160.9 ± 4.7%) (Figure 8, J and K). Our data thus suggest that mutation in σ_2-adaptin causes a BMP pathway-dependent aberrant NMJ morphology by altering the presynaptic cytoskeleton. We suggest that σ_2-adaptin-dependent endocytosis is essential for attenuating BMP-dependent synaptic growth signaling.

Discussion

AP2/CME has been proposed to play an essential role in SV endocytosis. Moreover, mutation in the proteins affecting CME also results in altered NMJ development in *Drosophila*, suggesting regulation of synaptic signaling by CME. In this study, we analyzed the role of AP2, one of the major adapters for clathrin at synapses, in the context of its physiological relevance and synaptic signaling. Our results demonstrate that AP2 facilitates basal synaptic transmission and SV endocytosis but also is essential during high-frequency nerve firing to regenerate SVs. Moreover, we provide evidence that AP2 regulates morphological plasticity at the *Drosophila* NMJ by

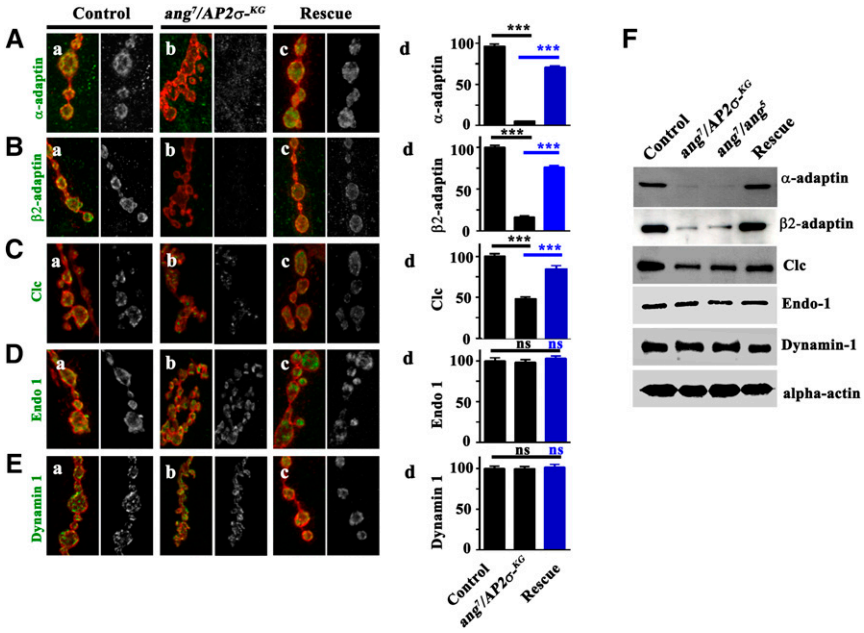

Figure 7 σ_2-adaptin is required specifically for AP2 complex and clathrin stability. (A–E) Representative images of third instar larval boutons from control, heteroallelic σ_2-*adaptin* mutant (*angur*^{7}/*AP2σ*^{KG02457}), and transgene-rescued (*actin5C/+*; *angur*^{7}/*UAS-AP2σ*, *AP2σ*^{KG02457}) NMJ synapses co-labeled with HRP (red) and other synaptic proteins (green): (A) α-adaptin; (B) β_2-adaptin; (C); EYFP-Clc (D) Endophilin 1, and (E) Dynamin 1. The histograms on the right show quantification of these synaptic proteins in the boutons, expressed as percentage of control levels. The fluorescence intensity of at least 50 individual boutons was measured and the background subtracted for the quantification. ***$P < 0.0001$. Error bars represent standard error of the mean. Statistical analysis based on one-way ANOVA followed by *post-hoc* Tukey's multiple-comparison test. (F) Western blot analysis of various synaptic proteins in larval brain of control, heteroallelic σ_2-*adaptin* mutant (*angur*^{7}/*AP2σ*^{KG02457} and *angur*^{7}/*angur*^{5}), and rescued animals (*actin5C/+*; *angur*^{7}/*UAS-AP2σ*, *AP2σ*^{KG02457}). Level of α-actin was used as loading control. The level of clathrin was assessed by probing the blots with anti-GFP antibody. For the EYFP-Clc experiment, the control genotype was *elav*^{C155}/+; *EYFP-Clc/+*; the heteroallelic mutant genotype was *elav*^{C155}/+; *EYFP-Clc/+*; *angur*^{7}/*AP2σ*^{KG02457}; and the rescue genotype was *elav*^{C155}/+; *EYFP-Clc/+*; *angur*^{7}/*UAS-AP2σ*, *AP2σ*^{KG02457}.

stabilizing the microtubule loops and attenuating the BMP signaling pathway.

Role of σ_2-adaptin in regulating rhabdomere biogenesis

The biogenesis of rhabdomeres is regulated by endocytosis and intracellular trafficking (Schuck and Simons 2004). Components of the endocytic machinery, when perturbed, lead to defects in rhabdomere formation. One such example is the disruption of the rhabdomere base when *shi*^{ts} flies are grown at restrictive temperature for 4 hr (Pinal and Pichaud 2011). Rh1-Gal4-driven *shi*^{ts1} flies raised at 19° led to an enlargement of photoreceptor cell bodies with the inter-rhabdomeric space being reduced (Gonzalez-Bellido *et al.* 2009). Similarly, when α-adaptin was knocked down using GMR-Gal4, rhabdomere biogenesis was disrupted, with smaller rhabdomeres (Raghu *et al.* 2009). In accordance with these observations, the TEM analysis of *angur* mutant eye clones showed no detectable rhabdomeres. Consistent with the defect in rhabdomere formation, we also observed no membrane depolarization in *angur* mutant eye clones. The visual cascade in *Drosophila* begins with rhodopsin being converted to meta-rhodopsin by light, followed by a subsequent phosphorylation by GPRK1. The phosphorylated meta-rhodopsin binds to arrestins, where its activity is quenched. The rhodopsin-arrestin complex is endocytosed, and rhodopsin is degraded in the lysosomes (Wang and Montell 2007). Thus, endocytosis regulates rhodopsin turnover in the photoreceptor cells, and blocking of the endocytic pathway components by mutations in Arr1, Arr2, or AP2 leads to retinal degeneration and photoreceptor cell death. This further establishes a strong link between endocytosis and retinal degeneration. Thus, it is likely that defective endocytosis in *angur* mutant eye clones affects meta-rhodopsin turnover, resulting into defective rhabdomeres and disorganized ommatidia. Moreover, endocytosis of several signaling receptors also has been shown to regulate morphogenesis during *Drosophila* eye development. The Notch signaling pathway has been studied extensively, and it has been shown that the Notch extracellular domain is transendocytosed during this process into the Delta-expressing cells (Weinmaster 2000). The localization of Notch and Delta is disrupted when endocytosis is acutely blocked, and this prevents internalization of Notch in the Delta-expressing cells (Parks *et al.* 2000). We thus speculate that the endocytic defect in *angur* mutant clones affects turnover and internalization of signaling molecules that may lead to defective rhabdomere development.

σ_2-adaptin regulates regeneration of SVs during high-frequency nerve firing

The functional analysis of the σ_2-*adaptin* mutants as well as of other subunits of AP2 reveals its requirement in maintaining basal synaptic transmission and regeneration of synaptic vesicles under high-frequency nerve firing at *Drosophila* NMJ synapses. Our data are consistent with previous reports showing the requirement for *Drosophila* α-adaptin in SV recycling at NMJ synapses (Gonzalez-Gaitan and Jackle 1997). However, in contrast to its role at mammalian central synapses, we found that loss of AP2 at *Drosophila* NMJ synapses affects basal synaptic transmission and SV endocytosis, albeit not very strongly. Moreover, the kinetics of SV re-formation in σ_2-*adaptin* mutants was only mildly affected. Consistent with the recent observation that loss of the AP2 complex at mammalian central synapses or its subunits in *C. elegans* affects synaptic vesicle biogenesis, we observed compromised synaptic transmission and SV

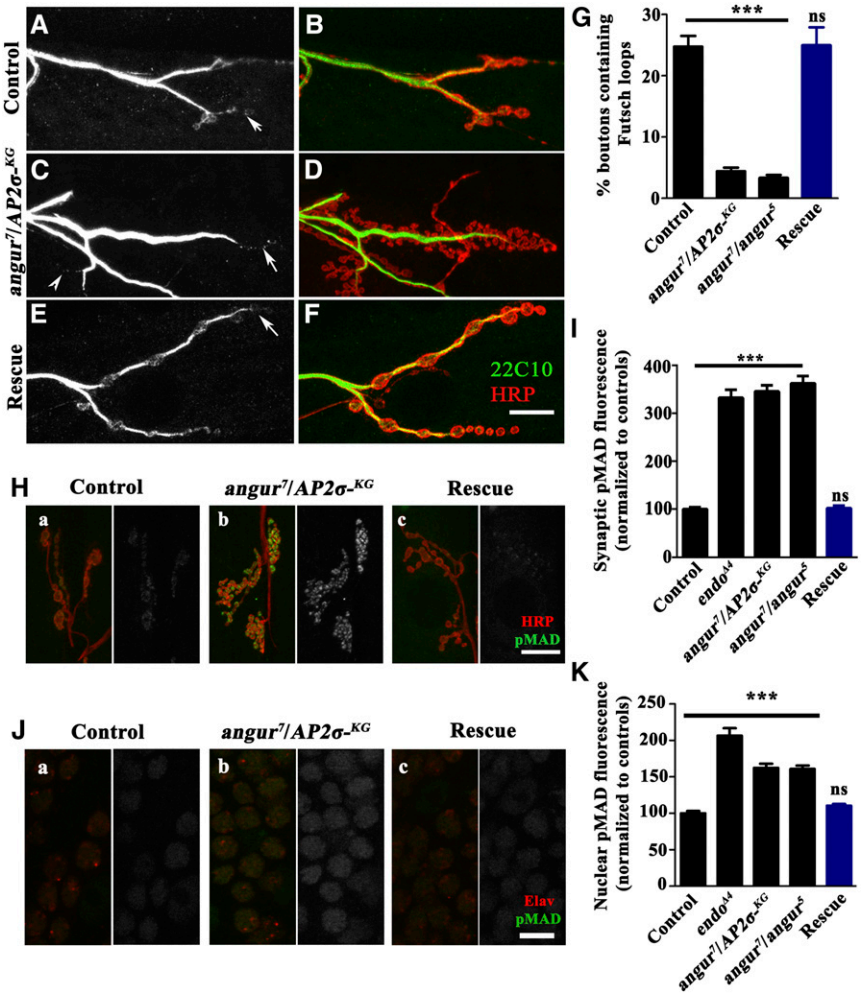

Figure 8 Mutations in σ_2-adaptin cause disruption of the presynaptic cytoskeleton and upregulated BMP signaling. (A–F) Representative images of third instar larval NMJs from (A and B) control animals, heteroallelic σ_2-*adaptin* mutants (C and D) (*angur*^{7}/*AP2σ*^{KG02457}), and transgene-rescued (E and F) (*actin5C/+*; *angur*^{7}*/UAS-AP2σ*, *AP2σ*^{KG02457}) animals co-labeled with HRP (red) and 22C10 (green). (G) Histogram showing quantification of the percentage of boutons containing Futsch loops of the indicated genotypes. ***$P < 0.0001$. Error bars represent standard error of the mean. Statistical analysis based on one-way ANOVA followed by *post-hoc* Tukey's multiple-comparison test. n = 6 NMJ synapses of muscles 6/7 of the A2 hemisegment. (H) Representative images of third instar larval boutons from (a) control, (b) heteroallelic σ_2-*adaptin* mutant (*angur*^{7}*/AP2σ*^{KG02457}), and (c) transgene-rescued (*actin5C/+*; *angur*^{7}*/UAS-AP2σ*, *AP2σ*^{KG02457}) NMJ synapses co-labeled with HRP (red) and pMAD (green). (I) Histogram showing quantification of synaptic pMAD fluorescence of the indicated genotypes. The fluorescence intensity of at least 50 individual boutons was measured and the background subtracted for the quantification.***$P <$ 0.0001. Error bars represent standard error of the mean. Statistical analysis based on one-way ANOVA followed by *post-hoc* Tukey's multiple-comparison test. (J) Representative images of motor nuclei of third instar larval VNC from (a) control, (b) heteroallelic σ_2-*adaptin* mutant (*angur*^{7}*/AP2σ*^{KG02457}), and (c) transgene-rescued (*actin5C/+*; *angur*^{7}*/UAS-AP2σ*, *AP2σ*^{KG02457}) animals co-labeled with Elav (red) and pMAD (green). (K) Histogram showing quantification of the nuclear pMAD fluorescence of the indicated genotypes. The fluorescence intensities of at least 50 motor nuclei were measured both for Elav and for pMAD, and the ratio of pMAD/elav represented in the quantification. ***$P < 0.0001$. Error bars represent standard error of the mean. Statistical analysis based on one-way ANOVA followed by *post-hoc* Tukey's multiple-comparison test.

re-formation after high-frequency stimulation, suggesting that at *Drosophila* NMJ synapses, AP2 function is required not only for SV trafficking but also for SV regeneration under high-frequency nerve stimulation (Gu *et al.* 2013; Kononenko *et al.* 2014). Our direct estimation of vesicle pool size in σ_2-*adaptin* mutants further supports its requirement in the regulation of SV pool size and is consistent with a recent report (Gu *et al.* 2013). Because loss of AP2 in *Drosophila* does not completely abrogate SV re-formation, it remains possible that other known synaptic clathrin adapters such as AP180, Eps15, and Epsin might partially compensate for loss of the AP2 complex (Zhang *et al.* 1998; Jakobsson *et al.* 2008; Cheung and Cousin 2012). This is corroborated by the observation that even a 96% reduction in synaptic α-adaptin level caused only an ~50% reduction in clathrin, suggesting that other clathrin adapters might contribute to retention and/or stability of synaptic clathrin.

The striking physiological defect in σ_2-*adaptin* mutants or neuronally reduced α-adaptin was their inability to recover from synaptic depression even after 4 min of cessation of high-frequency stimulation. Consistent with these observations, the endo-exo cycling pool did not recover to its initial value even after 4 min of rest following high-frequency nerve stimulation. This suggests that in addition to its requirement in synaptic vesicle endocytosis, AP2 complex functions at a relatively slower step downstream of membrane retrieval, possibly during membrane sorting from endosomes to regenerate fusion-competent synaptic vesicles (Gu *et al.* 2013; Kononenko *et al.* 2014).

PI(4,5)P2 and subunits of the AP2 complex are obligate partners for synapse growth in Drosophila

Several studies in cell culture support a model that indicates that the AP2 complex is an obligate heterotetramer for subunit stability and function (Motley *et al.* 2003; Boucrot *et al.* 2010). However, studies of AP2 function in *C. elegans* suggest that α/σ_2 subunits and β_2/μ_2 subunits may constitute two hemicomplexes that can carry out the minimal function of the

AP2 complex independent of one another (Gu *et al.* 2013). Does AP2 in *Drosophila* form hemicomplexes and contribute to vesicle trafficking? Our results do not support this model for *Drosophila*. First, unlike *C. elegans*, in which individual mutants for subunits of the AP2 complex are viable, the *Drosophila* mutant for α-adaptin is early larval lethal (Gonzalez-Gaitan and Jackle 1997). Consistent with these findings, neuronal knockdown of α-adaptin or β_2-adaptin resulted in third instar lethality. Second, if the hemicomplexes were functional in *Drosophila*, one would observe significant levels of synaptic β_2-adaptin in α-adaptin knockdown or *σ_2-adaptin* mutants. However, we observed that removing any of the subunits of the *Drosophila* AP2 complex in neurons resulted into an unstable AP2 complex and degradation of α− and β_2-adaptins. Third, inhibiting AP2 complex assembly by reducing synaptic PI(4,5)P2 levels also resulted into an unstable AP2 complex. These observations strongly suggest that in contrast to *C. elegans*, all the subunits of AP2 in *Drosophila* are obligate partners for a stable AP2 complex for clathrin-dependent SV trafficking.

Mutations in genes implicated in regulating CME, BMP signaling, or actin cytoskeleton dynamics all show abnormal NMJ development in *Drosophila*, characterized by either supernumerary boutons or an increased number but smaller boutons (Dickman *et al.* 2006; Wang *et al.* 2007; O'Connor-Giles *et al.* 2008; Nahm *et al.* 2013). The NMJ phenotype due to loss of σ_2-adaptin is consistent with that of other known endocytic mutants implicated in CME. The contrasting synaptic overgrowth observed in *σ_2-adaptin* mutants suggests a role for AP2 in mediating presynaptic growth signaling. Such synaptic overgrowth also was observed when any of the subunits of AP2 were downregulated or its assembly was interfered with by downregulating neuronal PI(4,5)P2. This suggests a pathway in which PI(4,5)P2 and the AP2 complex interact obligatorily to regulate synapse growth. The NMJ phenotype in *angur* mutants is strikingly more severe from that of the other synaptic mutants and points toward multiple growth signaling pathways that are possibly affected by an AP2-dependent endocytic deficit.

The abnormal synapse morphology in angur mutants is a consequence of alteration of the neuronal cytoskeleton

The morphology of the synapse is a consequence of the neuronal cytoskeleton network that shapes the growing synapse. Futsch, a protein with MAP1B homology, regulates the synaptic microtubule cytoskeleton, thereby controlling synaptic growth at the *Drosophila* NMJ (Roos *et al.* 2000). The hypothesis that the microtubule organization could be altered was strengthened by the dramatic decrease in the number of Futsch-positive loops in the *σ_2-adaptin* mutants. Futsch-positive loops have long been known to be associated with stable synaptic boutons, while the absence or disruption of these loops is indicative of boutons undergoing division or sprouting. The dramatic increase in the number of boutons in these mutants with a corresponding decrease in the number of loops correlates well with the fact that these boutons might be undergoing division. The phenotype associated with *futsch* mutants is fewer and larger boutons with impaired microtubule organization, which is an expected phenotype when bouton division is impaired. The *σ_2-adaptin* mutants, however, show a larger number but smaller-sized boutons, indicating that bouton division is enhanced. One of the signaling events that has been shown to dictate this process is BMP signaling (Wang *et al.* 2007). Further, BMP signaling is also required during developmental synaptic growth (Aberle *et al.* 2002; Marques *et al.* 2002; McCabe *et al.* 2003). Consistent with this, we found elevated pMAD levels in *σ_2-adaptin* mutants, indicating that BMP signaling is upregulated in these mutants. It has also been demonstrated that BMP signaling plays a role in maintenance of the presynaptic microtubule network (Wang *et al.* 2007). *Drosophila spichthyin* and *spartin* mutants have upregulated BMP signaling with significantly increased microtubule loops. It has been proposed that Futsch acts downstream of BMP signaling to regulate synaptic growth (Wang *et al.* 2007; Nahm *et al.* 2013). The *σ_2-adaptin* mutants also show upregulated BMP signaling, but in contrast to *spichthyin* and *spartin* mutants, *σ_2-adaptin* mutants have fewer Futsch loops, which also appeared fragmented. This suggests that deregulated BMP signaling, whether upregulation or downregulation, impairs microtubule stability. *dap160* mutants also show supernumerary boutons, with fragmented Futsch staining suggesting that the microtubule dynamics are misregulated in these mutants. Interestingly, Nwk levels are drastically altered in *dap160* mutants, suggesting that Nwk levels are important for maintaining microtubule stability (Koh *et al.* 2004). Because *σ_2-adaptin* mutants have normal Nwk levels, the observed synaptic overgrowth is independent of Nwk and suggests regulation of Futsch through Nwk-independent pathways.

Acknowledgments

We thank Hugo Bellen, Barry Ganetzky, and Peter Dijke for sharing antibodies and the Bloomington Drosophila Stock Center and Hybridoma Bank, University of Iowa, for fly lines and monoclonal antibodies. We thank Abdul Rahim Mohammad and Aseem Shrivastava for their help with initial characterization of the mutant and RNAi lines used in this study. We thank Seema Shirolikar, Lalit C. Borde, and Krishanu Ray (TIFR, Mumbai) for help with TEM. We thank Praveen Verma, NIPGR, New Delhi, for help with SEM. We thank Subhabrata Sanyal, Susy Kim, and Shanker Jha for many useful comments on the manuscript. This work was supported by project grants from the Department of Biotechnology, Government of India, to V.K. We thank IISER Bhopal for generous intramural funds and the Central Instrumentation Facility at IISER Bhopal.

Literature Cited

Aberle, H., A. P. Haghighi, R. D. Fetter, B. D. McCabe, T. R. Magalhaes *et al.*, 2002 *wishful thinking* encodes a BMP type II receptor that regulates synaptic growth in *Drosophila*. Neuron 33: 545–558.

Boucrot, E., S. Saffarian, R. Zhang, and T. Kirchhausen, 2010 Roles of AP-2 in clathrin-mediated endocytosis. PLoS One 5: e10597.
Brand, A. H., and N. Perrimon, 1993 Targeted gene expression as a means of altering cell fates and generating dominant phenotypes. Development 118: 401–415.
Cheung, G., and M. A. Cousin, 2012 Adaptor protein complexes 1 and 3 are essential for generation of synaptic vesicles from activity-dependent bulk endosomes. J. Neurosci. 32: 6014–6023.
Cheung, G., O. J. Jupp, and M. A. Cousin, 2010 Activity-dependent bulk endocytosis and clathrin-dependent endocytosis replenish specific synaptic vesicle pools in central nerve terminals. J. Neurosci. 30: 8151–8161.
Collins, B. M., A. J. McCoy, H. M. Kent, P. R. Evans, and D. J. Owen, 2002 Molecular architecture and functional model of the endocytic AP2 complex. Cell 109: 523–535.
Coyle, I. P., Y. H. Koh, W. C. Lee, J. Slind, T. Fergestad *et al.*, 2004 Nervous wreck, an SH3 adaptor protein that interacts with Wsp, regulates synaptic growth in *Drosophila*. Neuron 41: 521–534.
Delgado, R., C. Maureira, C. Oliva, Y. Kidokoro, and P. Labarca, 2000 Size of vesicle pools, rates of mobilization, and recycling at neuromuscular synapses of a *Drosophila* mutant, *shibire*. Neuron 28: 941–953.
Dickman, D. K., J. A. Horne, I. A. Meinertzhagen, and T. L. Schwarz, 2005 A slowed classical pathway rather than kiss-and-run mediates endocytosis at synapses lacking synaptojanin and endophilin. Cell 123: 521–533.
Dickman, D. K., Z. Lu, I. A. Meinertzhagen, and T. L. Schwarz, 2006 Altered synaptic development and active zone spacing in endocytosis mutants. Curr. Biol. 16: 591–598.
Dittman, J., and T. A. Ryan, 2009 Molecular circuitry of endocytosis at nerve terminals. Annu. Rev. Cell Dev. Biol. 25: 133–160.
Estes, P. S., J. Roos, A. van der Bliek, R. B. Kelly, K. S. Krishnan *et al.*, 1996 Traffic of dynamin within individual *Drosophila* synaptic boutons relative to compartment-specific markers. J. Neurosci. 16: 5443–5456.
Gonzalez-Bellido, P. T., T. J. Wardill, R. Kostyleva, I. A. Meinertzhagen, and M. Juusola, 2009 Overexpressing temperature-sensitive dynamin decelerates phototransduction and bundles microtubules in *Drosophila* photoreceptors. J. Neurosci. 29: 14199–14210.
Gonzalez-Gaitan, M., and H. Jackle, 1997 Role of Drosophila alpha-adaptin in presynaptic vesicle recycling. Cell 88: 767–776.
Granseth, B., B. Odermatt, S. J. Royle, and L. Lagnado, 2006 Clathrin-mediated endocytosis is the dominant mechanism of vesicle retrieval at hippocampal synapses. Neuron 51: 773–786.
Granseth, B., B. Odermatt, S. J. Royle, and L. Lagnado, 2007 Clathrin-mediated endocytosis: the physiological mechanism of vesicle retrieval at hippocampal synapses. J. Physiol. 585: 681–686.
Gu, M., Q. Liu, S. Watanabe, L. Sun, G. Hollopeter *et al.*, 2013 AP2 hemicomplexes contribute independently to synaptic vesicle endocytosis. eLife 2: e00190.
Heerssen, H., R. D. Fetter, and G. W. Davis, 2008 Clathrin dependence of synaptic-vesicle formation at the *Drosophila* neuromuscular junction. Curr. Biol. 18: 401–409.
Heuser, J. E., and T. S. Reese, 1973 Evidence for recycling of synaptic vesicle membrane during transmitter release at the frog neuromuscular junction. J. Cell Biol. 57: 315–344.
Jahn, R., and T. C. Sudhof, 1994 Synaptic vesicles and exocytosis. Annu. Rev. Neurosci. 17: 219–246.
Jakobsson, J., H. Gad, F. Andersson, P. Low, O. Shupliakov *et al.*, 2008 Role of epsin 1 in synaptic vesicle endocytosis. Proc. Natl. Acad. Sci. USA 105: 6445–6450.
Kim, S. H., and T. A. Ryan, 2009 Synaptic vesicle recycling at CNS snapses without AP-2. J. Neurosci. 29: 3865–3874.
Kim, S. M., V. Kumar, Y. Q. Lin, S. Karunanithi, and M. Ramaswami, 2009 Fos and Jun potentiate individual release sites and mobilize the reserve synaptic vesicle pool at the *Drosophila* larval motor synapse. Proc. Natl. Acad. Sci. USA 106: 4000–4005.
Koh, T. W., P. Verstreken, and H. J. Bellen, 2004 Dap160/intersectin acts as a stabilizing scaffold required for synaptic development and vesicle endocytosis. Neuron 43: 193–205.
Koh, T. W., V. I. Korolchuk, Y. P. Wairkar, W. Jiao, E. Evergren *et al.*, 2007 Eps15 and Dap160 control synaptic vesicle membrane retrieval and synapse development. J. Cell Biol. 178: 309–322.
Kononenko, N. L., D. Puchkov, G. A. Classen, A. M. Walter, A. Pechstein *et al.*, 2014 Clathrin/AP-2 mediate synaptic vesicle reformation from endosome-like vacuoles but are not essential for membrane retrieval at central synapses. Neuron 82: 981–988.
Kosaka, T., and K. Ikeda, 1983 Possible temperature-dependent blockage of synaptic vesicle recycling induced by a single gene mutation in *Drosophila*. J. Neurobiol. 14: 207–225.
Kumar, V., S. R. Alla, K. S. Krishnan, and M. Ramaswami, 2009 Syndapin is dispensable for synaptic vesicle endocytosis at the *Drosophila* larval neuromuscular junction. Mol. Cell. Neurosci. 40: 234–241.
Lakhotia, S. C., M. Mallik, A. K. Singh, and M. Ray, 2012 The large noncoding hsrω-n transcripts are essential for thermotolerance and remobilization of hnRNPs, HP1 and RNA polymerase II during recovery from heat shock in Drosophila. Chromosoma 121: 49–70.
Marie, B., S. T. Sweeney, K. E. Poskanzer, J. Roos, R. B. Kelly *et al.*, 2004 Dap160/intersectin scaffolds the periactive zone to achieve high-fidelity endocytosis and normal synaptic growth. Neuron 43: 207–219.
Marques, G., H. Bao, T. E. Haerry, M. J. Shimell, P. Duchek *et al.*, 2002 The *Drosophila* BMP type II receptor Wishful Thinking regulates neuromuscular synapse morphology and function. Neuron 33: 529–543.
Matsui, W., and T. Kirchhausen, 1990 Stabilization of clathrin coats by the core of the clathrin-associated protein complex AP-2. Biochemistry 29: 10791–10798.
McCabe, B. D., G. Marques, A. P. Haghighi, R. D. Fetter, M. L. Crotty *et al.*, 2003 The BMP homolog Gbb provides a retrograde signal that regulates synaptic growth at the *Drosophila* neuromuscular junction. Neuron 39: 241–254.
McMahon, H. T., and E. Boucrot, 2011 Molecular mechanism and physiological functions of clathrin-mediated endocytosis. Nat. Rev. Mol. Cell Biol. 12: 517–533.
Meinertzhagen, I. A., 1996 Ultrastructure and quantification of synapses in the insect nervous system. J. Neurosci. Methods 69: 59–73.
Motley, A., N. A. Bright, M. N. Seaman, and M. S. Robinson, 2003 Clathrin-mediated endocytosis in AP-2-depleted cells. J. Cell Biol. 162: 909–918.
Nahm, M., M. J. Lee, W. Parkinson, M. Lee, H. Kim *et al.*, 2013 Spartin regulates synaptic growth and neuronal survival by inhibiting BMP-mediated microtubule stabilization. Neuron 77: 680–695.
O'Connor-Giles, K. M., L. L. Ho, and B. Ganetzky, 2008 Nervous wreck interacts with thickveins and the endocytic machinery to attenuate retrograde BMP signaling during synaptic growth. Neuron 58: 507–518.
Parks, A. L., K. M. Klueg, J. R. Stout, and M. A. Muskavitch, 2000 Ligand endocytosis drives receptor dissociation and activation in the Notch pathway. Development 127: 1373–1385.
Persson, U., H. Izumi, S. Souchelnytskyi, S. Itoh, S. Grimsby *et al.*, 1998 The L45 loop in type I receptors for TGF-beta family

members is a critical determinant in specifying Smad isoform activation. FEBS Lett. 434: 83–87.
Pinal, N., and F. Pichaud, 2011 Dynamin- and Rab5-dependent endocytosis is required to prevent *Drosophila* photoreceptor degeneration. J. Cell Sci. 124: 1564–1570.
Poskanzer, K. E., R. D. Fetter, and G. W. Davis, 2006 Discrete residues in the c(2)b domain of synaptotagmin I independently specify endocytic rate and synaptic vesicle size. Neuron 50: 49–62.
Raghu, P., E. Coessens, M. Manifava, P. Georgiev, T. Pettitt *et al.*, 2009 Rhabdomere biogenesis in *Drosophila* photoreceptors is acutely sensitive to phosphatidic acid levels. J. Cell Biol. 185: 129–145.
Ramaswami, M., S. Rao, A. van der Bliek, R. B. Kelly, and K. S. Krishnan, 1993 Genetic studies on dynamin function in *Drosophila*. J. Neurogenet. 9: 73–87.
Ramaswami, M., K. S. Krishnan, and R. B. Kelly, 1994 Intermediates in synaptic vesicle recycling revealed by optical imaging of Drosophila neuromuscular junctions. Neuron 13: 363–375.
Rikhy, R., V. Kumar, R. Mittal, and K. S. Krishnan, 2002 Endophilin is critically required for synapse formation and function in *Drosophila melanogaster*. J. Neurosci. 22: 7478–7484.
Roos, J., and R. B. Kelly, 1998 Dap160, a neural-specific Eps15 homology and multiple SH3 domain-containing protein that interacts with *Drosophila* dynamin. J. Biol. Chem. 273: 19108–19119.
Roos, J., T. Hummel, N. Ng, C. Klambt, and G. W. Davis, 2000 *Drosophila* Futsch regulates synaptic microtubule organization and is necessary for synaptic growth. Neuron 26: 371–382.
Ruiz-Canada, C., J. Ashley, S. Moeckel-Cole, E. Drier, J. Yin *et al.*, 2004 New synaptic bouton formation is disrupted by misregulation of microtubule stability in aPKC mutants. Neuron 42: 567–580.
Saheki, Y., and P. De Camilli, 2012 Synaptic vesicle endocytosis. Cold Spring Harb. Perspect. Biol. 4: a005645.
Sato, K., G. G. Ernstrom, S. Watanabe, R. M. Weimer, C. H. Chen *et al.*, 2009 Differential requirements for clathrin in receptor-mediated endocytosis and maintenance of synaptic vesicle pools. Proc. Natl. Acad. Sci. USA 106: 1139–1144.
Schmid, E. M., and H. T. McMahon, 2007 Integrating molecular and network biology to decode endocytosis. Nature 448: 883–888.
Schuck, S., and K. Simons, 2004 Polarized sorting in epithelial cells: raft clustering and the biogenesis of the apical membrane. J. Cell Sci. 117: 5955–5964.
Sengupta, S., and S. C. Lakhotia, 2006 Altered expressions of the noncoding *hsrω* gene enhances poly-Q-induced neurotoxicity in *Drosophila*. RNA Biol. 3: 28–35.
Song, W., and K. E. Zinsmaier, 2003 Endophilin and synaptojanin hook up to promote synaptic vesicle endocytosis. Neuron 40: 665–667.
Stimson, D. T., P. S. Estes, S. Rao, K. S. Krishnan, L. E. Kelly *et al.*, 2001 *Drosophila* stoned proteins regulate the rate and fidelity of synaptic vesicle internalization. J. Neurosci. 21: 3034–3044.
Stowers, R. S., and T. L. Schwarz, 1999 A genetic method for generating Drosophila eyes composed exclusively of mitotic clones of a single genotype. Genetics 152: 1631–1639.
Traub, L. M., 2003 Sorting it out: AP-2 and alternate clathrin adaptors in endocytic cargo selection. J. Cell Biol. 163: 203–208.
Vanlandingham, P. A., T. R. Fore, L. R. Chastain, S. M. Royer, H. Bao *et al.*, 2013 Epsin 1 promotes synaptic growth by enhancing BMP signal levels in motoneuron nuclei. PLoS One 8: e65997.
Verstreken, P., O. Kjaerulff, T. E. Lloyd, R. Atkinson, Y. Zhou *et al.*, 2002 Endophilin mutations block clathrin-mediated endocytosis but not neurotransmitter release. Cell 109: 101–112.
Wang, T., and C. Montell, 2007 Phototransduction and retinal degeneration in *Drosophila*. Pflugers Arch. 454: 821–847.
Wang, X., W. R. Shaw, H. T. Tsang, E. Reid, and C. J. O'Kane, 2007 *Drosophila* spichthyin inhibits BMP signaling and regulates synaptic growth and axonal microtubules. Nat. Neurosci. 10: 177–185.
Watanabe, S., T. Trimbuch, M. Camacho-Perez, B. R. Rost, B. Brokowski *et al.*, 2014 Clathrin regenerates synaptic vesicles from endosomes. Nature 515: 228–233.
Weinmaster, G., 2000 Notch signal transduction: a real rip and more. Curr. Opin. Genet. Dev. 10: 363–369.
Wolff, T., 2011 Preparation of Drosophila eye specimens for scanning electron microscopy. Cold Spring Harb. Protoc. 2011: 1383–1385.
Zhang, B., Y. H. Koh, R. B. Beckstead, V. Budnik, B. Ganetzky *et al.*, 1998 Synaptic vesicle size and number are regulated by a clathrin adaptor protein required for endocytosis. Neuron 21: 1465–1475.
Zinsmaier, K. E., K. K. Eberle, E. Buchner, N. Walter, and S. Benzer, 1994 Paralysis and early death in cysteine string protein mutants of Drosophila. Science 263: 977–980.

Communicating editor: R. J. Duronio

GENETICS

Supporting Information
www.genetics.org/lookup/suppl/doi:10.1534/genetics.115.183863/-/DC1

σ_2-Adaptin Facilitates Basal Synaptic Transmission and Is Required for Regenerating Endo-Exo Cycling Pool Under High-Frequency Nerve Stimulation in *Drosophila*

Saumitra Dey Choudhury, Zeeshan Mushtaq, Suneel Reddy-Alla, Sruthi S. Balakrishnan, Rajan S. Thakur, Kozhalmannom S. Krishnan, Padinjat Raghu, Mani Ramaswami, and Vimlesh Kumar

DOI: 10.1534/genetics.115.183863

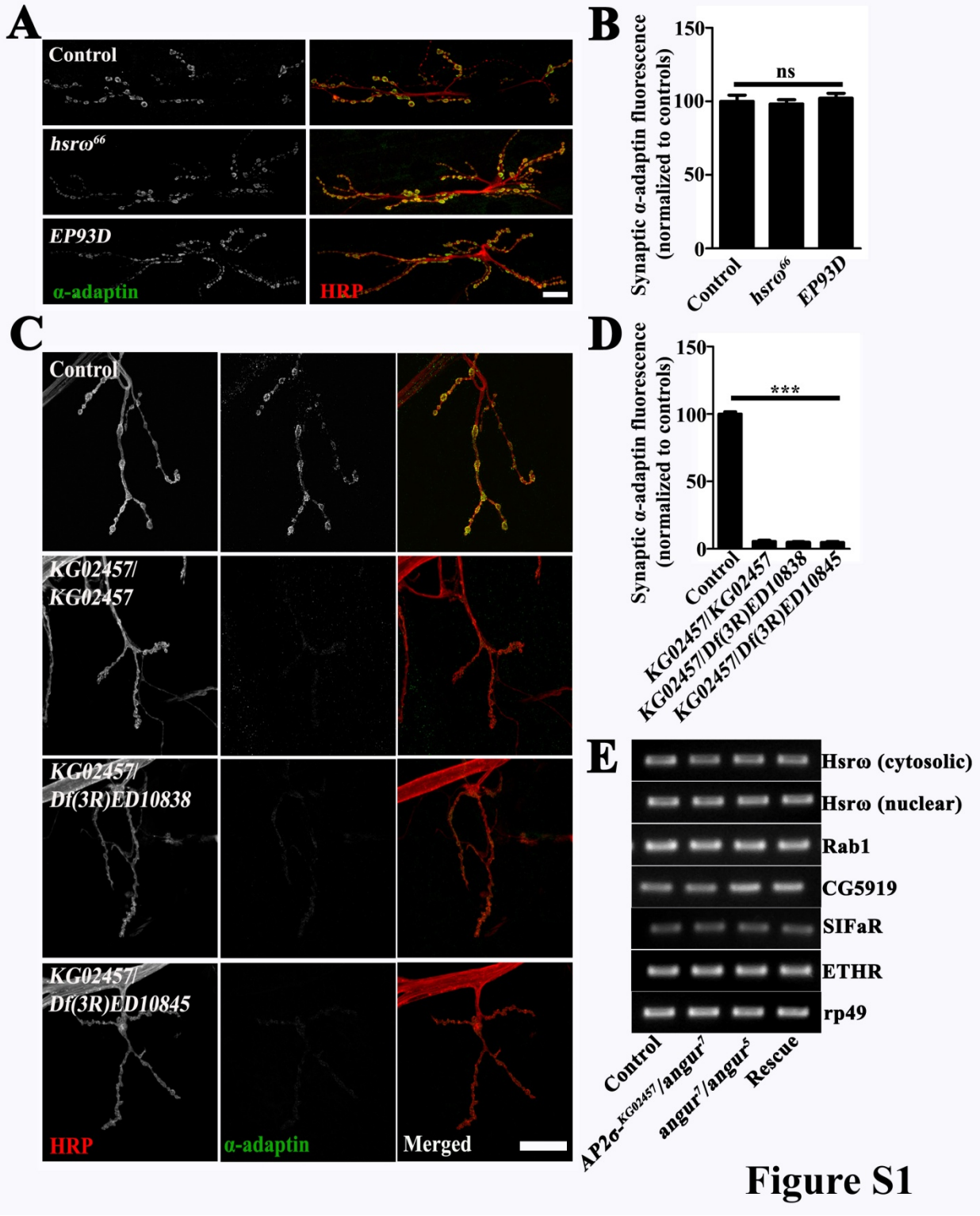

Figure S1

Figure S1. The P-element insertions in *angur* mutants upstream of *hsrω* specifically affects σ_2-adaptin while *hsrw* mutants do not affect σ_2-adaptin

(A) Confocal images of NMJ synapses at muscle 6/7 colabelled with α-adaptin (green) and HRP (red) of control, *hsrω*^{66} and *EP93D*. Note that α-adaptin levels are unaltered in these mutants. Scale bar represents 15 μm.

(B) Histogram showing quantification of synaptic α-adaptin in control, *hsrω*^{66} and *EP93D*. The fluorescence intensity of 30 individual boutons was measured and the background subtracted for the quantification. *** represents $p<0.0001$. Error bars represent standard error of the mean (SEM). Statistical analysis based on one-way ANOVA followed by post-hoc Tukey's multiple comparison test.

(C) Confocal images of NMJ synapses at muscle 4 colabelled with α-adaptin (green) and HRP (red) of control, homozygous *AP2σ*-^{KG02457} animals and heteroallelic combination with deficiencies (*AP2σ*-^{KG02457}/Df(3R)ED10838 and *AP2σ*-^{KG02457}/Df(3R)ED10845). Note that both these allelic combinations phenocopies *angur* mutation with a severe reduction in synaptic α-adaptin. Scale bar represents 25 μm.

(D) Histogram showing quantification of synaptic α-adaptin in control, homozygous *AP2σ*-^{KG02457}, *AP2σ*-^{KG02457}/Df(3R)ED10838 and *AP2σ*-^{KG02457}/Df(3R)ED10845. The fluorescence intensity of 30 individual boutons was measured and the background subtracted for the quantification. *** represents $p<0.0001$. Error bars represent standard error of the mean (SEM). Statistical analysis based on one-way ANOVA followed by post-hoc Tukey's multiple comparison test.

(E) Semi-quantitative RT-PCR showing transcript levels of Hsrω (cytosolic), Hsrω (nuclear), Rab1, CG5919, SIFaR and ETHR in controls, *angur*^{7}/ *AP2σ*^{KG02457}, *angur*^{7} /*angur*^{5} and rescued heteroallelic mutant (*actin5C*/+; *angur*^{7} /UAS-AP2σ , *AP2σ*^{KG02457}) respectively. Hsrω (cytosolic), Hsrω (nuclear), Rab1, CG5919, SIFaR and ETHR transcript levels were not altered in any of these genotypes. *rp49* transcript level was used as an internal concentration control for mRNA.

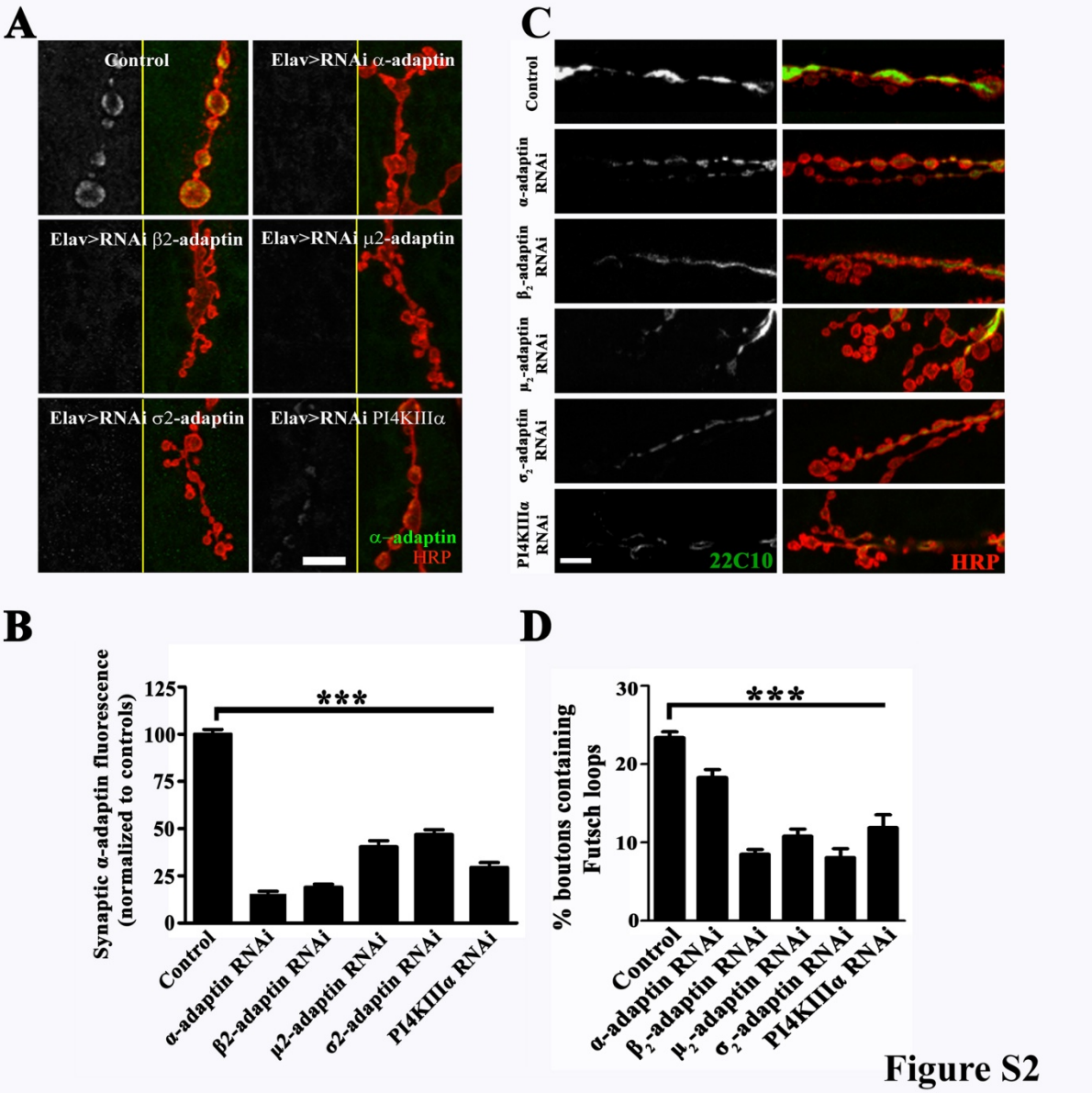

Figure S2

Figure S2. RNAi-mediated knockdown of AP2 subunits phenocopies σ_2-adaptin mutation and destabilizes AP2 complex

(**A**) Confocal images of NMJ boutons colabelled with HRP (red) and α-adaptin (green) of control and neuronally expressing RNAi against AP2 subunits; α-adaptin, β_2-adaptin, μ_2-adaptin, σ_2-adaptin or PI4KIIIα. Note that neuronal knockdown of any of the subunits phenocopies *σ_2-adaptin* mutants. Also it destabilises the AP2 complex as revealed by dramatic reduction of α-adaptin immunostaining. Scale bar represents 10 μm.

(**B**) Histogram showing quantification of synaptic α-adaptin in control and neuronally expressing RNAi against AP2 subunits or PI4KIIIα. The fluorescence intensity of at least 50 individual boutons was measured and the background subtracted for the quantification. *** represents $p<0.0001$. Error bars represent standard error of the mean (SEM). Statistical analysis based on one-way ANOVA followed by post-hoc Tukey's multiple comparison test.

(**C**) Confocal images of NMJ boutons colabelled with HRP (red) and 22C10 (green) of control and neuronally expressing RNAi against AP2 subunits; α-adaptin, β_2-adaptin, μ_2-adaptin, σ_2-adaptin or PI4KIIIα. Scale bar represents 5 μm.

(**D**) Histogram showing quantification of the percentage of boutons containing Futsch loops in control and neuronally expressing RNAi against AP2 subunits or PI4KIIIα. The number of Futsch loops in six NMJ synapses of muscle 6/7 of A2 hemisegment were counted. *** represents $p<0.0001$. Error bars represents standard error of the mean (SEM). Statistical analysis based on one-way ANOVA followed by post-hoc Tukey's multiple comparison test.

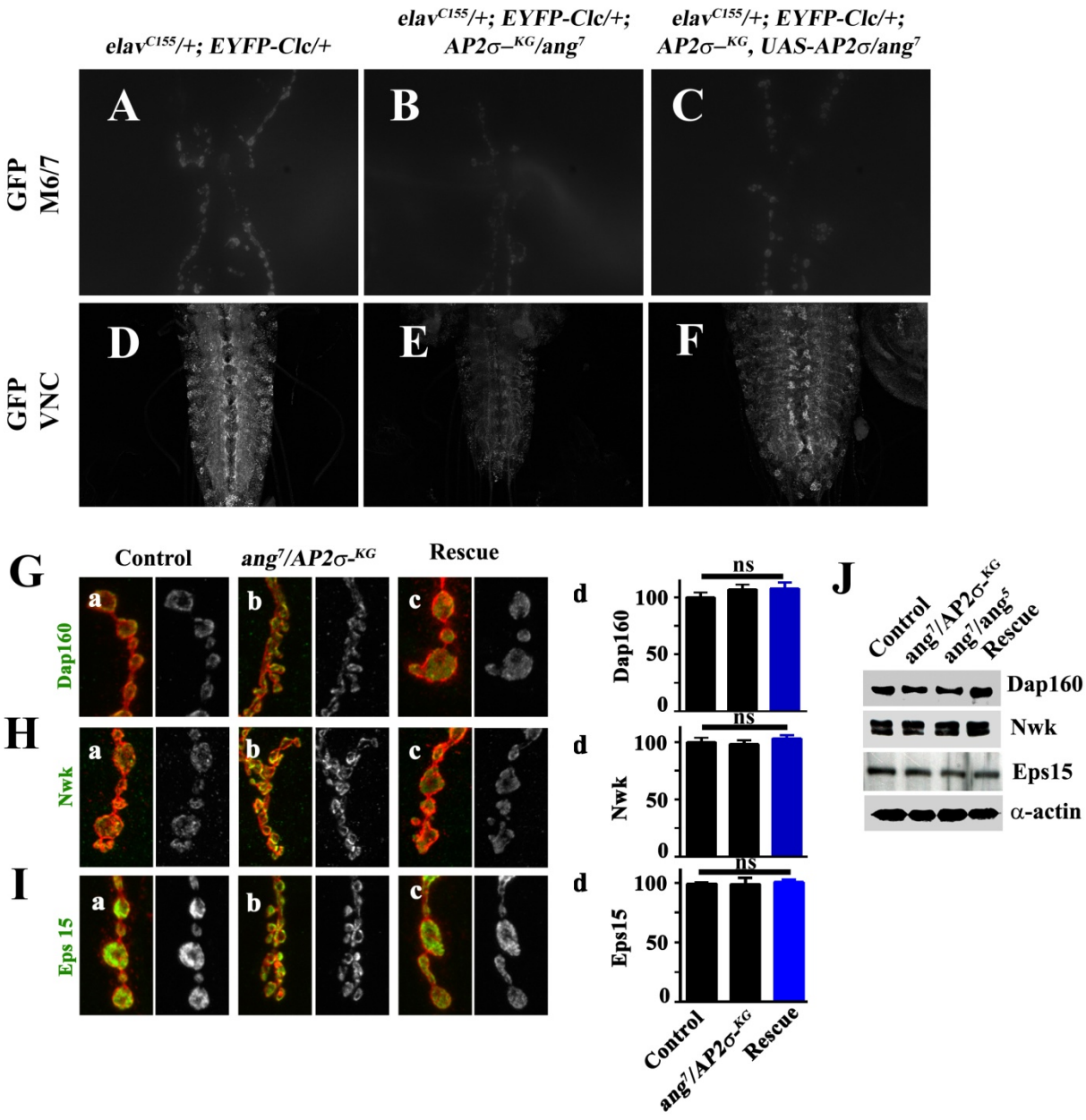

Figure S3

Figure S3. Reduced AP2 levels affect Clathrin stability

(**A-C**) Representative images of third instar larval NMJ synapses from control (*elav^{C155}*/+; *EYFP-Clc*/+), heteroallelic *σ$_2$-adaptin* mutant expressing EYFP-Clc in neurons (*elav^{C155}*/+; *EYFP-Clc*/+; *angur^{7}*/*AP2σ^{KG02457}*) and transgene rescued NMJ synapses coexpressing EYFP-Clc (*elav^{C155}*/+;*EYFP-Clc*/+;*AP2σ^{KG02457}*,*UAS-AP2σ*/*angur^{7}*).

(**D-F**) Representative images of ventral nerve cord of third instar larvae from control (*elav^{C155}*/+; *EYFP-Clc*/+), heteroallelic *σ$_2$-adaptin* mutant expressing EYFP-Clc in neurons (*elav^{C155}*/+; *EYFP-Clc*/+; *angur^{7}*/*AP2σ^{KG02457}*) and transgene rescued NMJ synapses coexpressing EYFP-Clc (*elav^{C155}*/+;*EYFP-Clc*/+; *AP2σ^{KG02457}*,*UAS-AP2σ*/*angur^{7}*).

(**G-I**) Representative images of third instar larval NMJ synapses from (a) control, (b) heteroallelic *σ$_2$-adaptin* mutant (*angur^{7}*/*AP2σ^{KG02457}*) and (c) rescued animals (*actin5C*/+; *angur^{7}*/*UAS-AP2σ, AP2σ^{KG02457}*) colabelled with HRP (red) and other synaptic proteins (green), (G) Dap160; (H) Nwk and (I) Eps15. The histograms in right (d) show quantification of these synaptic proteins in the boutons, expressed as percentage of control levels. The fluorescence intensity of at least 50 individual boutons was measured and the background subtracted for the quantification. The fluorescence intensity values of all genotypes are represented in Table S3.

Error bars represent standard error of the mean (SEM). Statistical analysis based on one-way ANOVA followed by post-hoc Tukey's multiple comparison test.

(**J**) Western blot analysis of various synaptic proteins in larval brain of wild-type, heteroallelic *σ$_2$-adaptin* mutants (*angur^{7}*/*AP2σ^{KG02457}* and *angur^{7}*/*angur^{5}*) and rescued animals (*actin5C*/+; *angur^{7}*/*UAS-AP2σ, AP2σ^{KG02457}*). Level of α-actin was used as loading control.

Table S1. Phenotypes obtained on knocking down the components of the AP2 complex or PI4KIIIα with various Gal4 drivers.

	RNAi α-adaptin (BL 32866)	**RNAi β_2-adaptin (BL 28328)**	**RNAi μ_2-adaptin (BL28040)**	**RNAi σ_2-adaptin (BL 27322)**	**RNAi PI4KIIIα (BL35256)**
eyeless Gal4	Headless phenotype in pupae	Headless phenotype in pupae	Normal eye	Range of eye phenotypes	Normal eye
actin5C Gal4	Lethal at 29^0C and 25^0C	Lethal at 29^0C and 25^0C	Lethal at 29^0C and 25^0C	Sluggish 3rd instar larvae which die	Lethal at 29^0C and 25^0C
elav^{C155} Gal4	Sluggish 3rd instar larvae (25^0C) which die	Active larvae but die as early pupae (25^0C)	Normal adults	Adults that paralyze at 37^0C	Sluggish 3rd instar larvae (25^0C) which die
D42 Gal4	Sluggish 3rd instar larvae (25^0C) which die	Active larvae but die as early pupae (25^0C)	Normal adults	Normal adults	Sluggish 3rd instar larvae (25^0C) which die
mef2 Gal4	Pupate but die before pharate adult	Pupate but die before pharate adult	Normal adults	Pupate but die before pharate adult if enhanced with *UAS-Dicer*	Pupate but die soon after

Table S2. Different primers with their sequences which were used for performing real time qPCR/semi-quantitative RT PCR in this study.

SL.NO.	PRIMER NAME	SEQUENCE
1.	AP2σ Forward	5’-CGCTATGCGGGTCTGTACTT-3’
2.	AP2σ Reverse	5’-CCAGGAACATCTCGTCCACC-3’
3.	Rab1 Forward	5’-GAGGAGATCGAGCGGTATGC-3’
4.	Rab1 Reverse	5’-ATCGTCATGAAGGCCTGCTC-3’
5.	CG5919 Forward	5’-TACCTGACCCGCATCCACTA-3’
6.	CG5919 Reverse	5’-GAGAGAACCAGGGTGTCAGC-3’
7.	rp49 Forward	5’- GCCGCTTCAAGGGACAGTAT-3’
8.	rp49 Reverse	5’-CTTGCGCTTCTTGGAGGAGA-3’
9.	ETHR Forward	5’-TTCTGTGGGTGGCCGAGTA-3’
10.	ETHR Reverse	5’- GCCCTGTTGGAGACCAGATT-3’
11.	SIFaR Forward	5’- CTCAAGAAGGTGATGCCGGT-3’
12.	SIFaR Reverse	5’- TGGTAGTGCGATGACTTCCG-3’
13.	Hsrω (Nuclear) Forward	5’- TCCGCATTTATTTTTCTCCAC-3’
14.	Hsrω (Nuclear) Reverse	5’- GTGTATAGAATTTGGGACCTCCA-3’
15.	Hsrω (Cytosolic) Forward	5’- TAGGAAGCCAGTGGGCGT-3’
16.	Hsrω (Cytosolic) Reverse	5’- CCGAGTGCGTTTTCAGCA-3’

The Hsrω primer sets were designed as previously described (COLLINGE *et al.* 2008).

REFERENCE:

COLLINGE, J. E., A. R. ANDERSON, A. R. WEEKS, T. K. JOHNSON and S. W. MCKECHNIE, 2008 Latitudinal and cold-tolerance variation associate with DNA repeat-number variation in the hsr-omega RNA gene of Drosophila melanogaster. Heredity (Edinb) **101:** 260-270.